Karapetrou, S., Manakou, M., Bindi, D., Petrovic, B., Pitilakis, K. (2016): “Time-building specific” seismic vulnerability assessment of a hospital RC building using field monitoring data. - *Engineering Structures*, *112*, pp. 114—132.

DOI: http://doi.org/10.1016/j.engstruct.2016.01.009

"Time-building specific" seismic vulnerability assessment of a hospital RC building using field monitoring data

S. Karapetrou[a,*], M. Manakou[a], D. Bindi[b], B. Petrovic[b] and K. Pitilakis[a]

[a] Aristotle University, Department of Civil Engineering, Research Unit of Geotechnical Earthquake Engineering and Soil Dynamics, Thessaloniki, Greece

[b] Helmoholtz Centre Potsdam GFZ German Research Centre For Geosciences, Potsdam, Germany

*Corresponding author: S. Karapetrou (gkarapet@civil.auth.gr, phone number: +30 2310 994208)

ABSTRACT

In the context of seismic vulnerability assessment of reinforced concrete (RC) buildings, the use of field monitoring data constitutes a significant tool for the representation of the actual structural state, reducing uncertainties associated with the building configuration properties as well as many non-physical parameters (age, maintenance, etc.), enhancing thus the reliability in the risk assessment procedure. In this study, the seismic vulnerability of existing RC buildings is evaluated, combining through a comprehensive methodology, the numerical analysis and field monitoring data. The proposed methodology is highlighted through the derivation of "time-building specific" fragility curves for an eight-storey RC structure (hospital building), built almost five decades ago, that is composed by two adjacent units connected with a structural joint. The assessment of the dynamic characteristics is performed using ambient noise measurements recorded by a temporary seismic network which was deployed inside the hospital. The modal identification results are used to update and better constrain the initial finite element model of the building, which is based on the available design and construction documentation plans. Three-dimensional incremental dynamic analysis is performed to derive the fragility curves for the initial as built model ("building-specific") and for the real structures as they are nowadays ("time-building specific"). The initial "building-specific" curves are evaluated through their comparison with conventional generic curves that are commonly used in risk assessment studies. Moreover, in order to enhance the reliability of the obtained results, the "time-building specific" fragility curves, are compared to time-dependent curves derived for the hospital units adopting an appropriate for the specific case study corrosion scenario. Results derived from both approaches indicate that the consideration of the actual state of structures may significantly alter their expected seismic performance leading to higher vulnerability values.

Keywords: Building monitoring; operational modal analysis; finite element updating; time-building specific vulnerability assessment; time-dependent fragility curves; incremental dynamic analyses; aging

1. INTRODUCTION

The devastating impacts from past seismic events have shown that prevention and preparedness are key tools for improving the seismic safety and resilience to earthquake disasters. Risk and vulnerability of urban sites to earthquake hazard lead to an emerging need for developing operational frameworks that can be used by the authorities (e.g. civil protection authorities, end users) in pre-crises situation to establish decision making procedures and risk mitigation strategies. In this context, the reliable vulnerability assessment of existing structures and infrastructures is a prerequisite for seismic loss estimation, risk mitigation and management.

Vulnerability is commonly expressed through fragility functions representing the probability of exceeding a prescribed damage limit state for a certain level of ground motion intensity. However, in seismic vulnerability assessment studies the common practice is to neglect the development of degradation phenomena in time, such as progressive deterioration of material properties, structural modifications or existing damages from previous earthquakes, which may adversely affect the capacity and seismic performance of structures with time. Recent studies investigated these effects on the structural response and fragility under dynamic loading, namely aging [1] and cumulative earthquake damage [2] proving that conventional generic fragility curves [3] may not accurately represent the actual state of existing structural systems but need to be updated in order to reflect their real condition. Moreover, uncertainties associated with the construction systems, material, mass and geometry properties that are pronounced particularly in the case of existing buildings may not be properly captured using generic fragility curves. Although widely applied seismic vulnerability assessment methods (e.g. HAZUS methodology) allow the integration of coefficients that depend on the maintenance condition or are related to in-situ properties of building materials, such integration does not necessarily increase the reliability of the results as the actual structural state may still not be captured properly. It should be noted herein that the above general statements and the related references are associated basically with large scale vulnerability assessment procedures (i.e. at urban/regional scale) while the paper is focused on a comprehensive methodology able to cover the need of seismic performance assessment of a single individual building taking into account aging of materials.

The use of field monitoring data for identifying the actual state of existing structures has recently drawn attention in civil engineering community for developing real time assessment tools and reducing uncertainties involved within the risk assessment procedure ([4], [5], [6]). Real-time monitoring of civil structures and infrastructures provide valuable information to assess the structural health and identify the actual state and vulnerability of the associated systems. Furthermore, it allows monitoring the evolution of the structure's safety during the

earthquake crisis while it constitutes the key component for rapid damage assessment or the preparation of reliable damage scenarios. In [7] an approach for robust evaluation and monitoring of instrumented buildings is proposed in the context of rapid post-earthquake emergency management. In [6] the main aim is to show how the experimental model extracted from ambient vibration measurements may contribute in the framework of seismic vulnerability assessment of existing buildings in moderate seismic-prone regions. The interest of scientific research as well as civil protection in the development of integrated suites of tools and methodologies to rapidly extract, collect and integrate information on the exposure of the urban environment to seismic risk is growing constantly not only in Europe but also worldwide. Currently research is concentrating on issues such as rapid damage detection of single important structures, rapid and reliable damage scenario preparation and early earthquake warning. On a building specific scale a permanent instrumentation array installed inside the building (especially in the case of structures/infrastructures with strategic interest) allows the development of a building-specific alert procedure suitable for performing an automated building tagging and the establishment of decision making strategies which will allow the Civil protection authorities to act efficiently in real (or near real-time) and after the event. The main goal is the fast assessment of structural health conditions in the early post-earthquake phase. The key issue for the implementation of an advanced seismic protection system requires reduction of the computational effort and the reaction time [8]. Automated identification procedures ([8], [9], [10], [11]) may contribute significantly in this direction allowing a fast evaluation of health conditions of a structure after an earthquake or during a seismic sequence. One of the advantages of the wireless units with embedded computing power is that they can be rapidly installed inside a building during a seismic sequence and, later, collect the data from outside through the wifi connection. An example is given in [12], where the Navelli city hall was damaged by the l'Aquila earthquake and later monitored with SOSEWIN instruments during the aftershocks sequence. Since the units have computing power, that is they can process the data and communicate the outcomes, software for damage detection can be installed in the firmware [13].

In this context, dynamic characterization of civil engineering structures (natural frequencies, damping ratios, mode shapes) using monitoring data becomes increasingly important in a wide range of research and application fields, such as dynamic response prediction (e.g. [14], [15]; [16]), finite element model updating (e.g. [15]; [16]; [17]; [18]; [19]; [20]; [21]; [22]), structural health monitoring (e.g. [23]) and damage detection ([24]; [25]; [26]; [27]). In order to predict or modify the response of a structure, an accurate well-known experimental modal model is required that represents the dynamics of the structure [28]. Rapid development of data acquisition and processing capabilities has given rise to major advances in the experimental operational studies and more specifically in the estimation of

modal parameters of vibrating systems. An experimental modal model of an artificially excited structure can be obtained based on Experimental Modal Analysis (EMA) by measuring the forces and vibrational structural responses ([29]; [30]; [31]). However, for large-scale applications (e.g. civil engineering structures) Operational Modal Analysis (OMA) is generally preferred to forced vibration measurements due to the fact that the same modal parameters can be obtained from vibration data in operational rather than laboratory conditions [32]. Ambient noise measurements are usually used to perform OMA and indentify the modal parameters of a structure.

In order to derive ”time-building specific” fragility curves based on field monitoring data, that represent the actual state and vulnerability of a structure, the measured modal parameters can be used to improve the finite element models to better reflect the measured data. The lack of correlation between the numerical structural models and experimental observations may be attributed to poorly known boundary conditions and material properties or modeling simplifications. Due to these uncertainties, the predicted analytical dynamics of an as built structure based on the initial design plans, may differ from the measured dynamics of the real structure.

In the present study an integrated methodology is presented for assessing the ”time-building-specific” seismic vulnerability of one of the main buildings of the most important hospital in Thessaloniki (AHEPA) based on field monitoring data. The AHEPA hospital has been selected as test site for the European funded project REAKT (http://www.reaktproject.eu/) for the development of an operational framework for rapid post-earthquake damage evaluation and risk assessment in real or near-real time. ”Time-building specific” vulnerability in this case refers to the present (actual) seismic vulnerability of the building considering all possible geometrical modifications, mass distributions and material deterioration. In Bindi et al. [33] a detailed and comprehensive study is presented regarding the dynamic characterization of the hospital building applying both vibrational and waveform approaches to identify the real structural conditions and potential pathology of the building. In the context of the vibrational approach the monitoring data are used to extract the modal parameters of the building based on operational modal analysis. In the present study, the modal identification results are used to update and better constrain the initial finite element model of the building, which is based on the design and construction documentation plans provided by the Technical Services of the hospital. For both initial (“building specific”) and updated (“time-building specific”) finite element models, three-dimensional nonlinear incremental dynamic analysis is performed to derive the fragility curves and evaluate the actual state of the hospital. The results are evaluated comparing the “building specific” curves with generic fragility curves [3], which are generated for representative structural typologies and are commonly used in the framework of loss assessment and risk

management studies. Furthermore the updated ("time-building specific") fragility curves are compared with the "time-dependent" curves of the hospital building that are extracted taking into account the impact of deterioration of the material properties with time (aging effects) following the analytical method proposed by Pitilakis et al. [1].

2. DESCRIPTION OF THE AHEPA HOSPITAL AND INSTRUMENTATION ARRAYS

The AHEPA hospital is located in the campus of Aristotle University of Thessaloniki. In case of the emergency its central location in the city of Thessaloniki makes it one of the most important medical care centers for an efficient crisis management. Due to its strategic interest it has been selected in the framework of the REAKT project (http://www.reaktproject.eu/) to generate real-time risk estimates and to optimize rapid post-earthquake response based on real and various scenario earthquakes. The target building hosts both administration and hospitalization activities. It was constructed in 1971 and is considered representative of structures that have been designed with low seismic code provisions ('Royal Decree' of 1959), where the ductility and the dynamic features of the constructions are ignored. During the 1978 Thessaloniki earthquake (M=6.5, R=26.7km, [34]; [35]), which generally caused extensive damages and the collapse of one high-rise residence structure, the hospital building suffered only slight damage. It is an eight-storey infilled moment resisting frame building and its special feature is that it is composed of two adjacent tall building units (namely UNIT 1 & UNIT 2) that are connected with a structural joint (Fig. 1a). UNIT 1 has a 29m × 16m rectangular plan section whereas UNIT 2 covers a trapezoidal section of 21m × 27m ×16m. The interstorey height is regular between the floor levels (3.4m) except for the second floor (4.8m). From the structural point of view the building's force resisting mechanism comprises longitudinal and externally transverse reinforced concrete moment resisting frames (Fig. 1a). The columns have variable dimensions along the height of the building starting from 0.45m x 0.70m at the lowest level (basement) and resulting to 0.35m x 0.35m at the upper floor. In the longitudinal direction the outer and inner columns are connected by beams with cross-section of 0.20m x 0.60m and 0.35m x 0.40m respectively. In the transverse direction on the other hand only the exterior columns are connected by beams with dimensions of 0.20m x 0.95m. The presence of beam to beam connections at all floor levels near the staircases and elevator shafts, constitute a complex structural system which is particularly evident in the middle floor where the RC beams are inverted. Reinforced concrete walls are present in both building units, surrounding partially the staircases and the lift shafts; they are not specially detailed for seismic performance. More specifically there are two walls in the transverse and one in the longitudinal direction of UNIT 1 and only one wall in the transverse direction of UNIT 2. The

RC walls are 0.20m thick while their length is decreasing significantly along the structure's height. Moreover a perimeter reinforced concrete wall with dimensions of 0.20m x 3.00m has been constructed at top of the building. Fig. 1b and Fig. 2a present the geometrical properties of the section and the reinforcement details of the elements respectively. Moreover Fig. 2b illustrates the diameters and position of the reinforced bars of walls and columns indicatively for the 1st and 2nd floor where the storey height is superior in relation to the other floors. In-situ testing on materials, structural details and non-structural components were not possible to be conducted. The material properties and the structural details used for the numerical modeling of the building units, are defined based on the information of the available blueprints as one of the main objectives of the present study is to investigate the effects of aging on the initial structural parameters. More specifically concrete B225 (f_c=14MPa) is used for all beams and columns while two steel classes StIII (f_y=500MPa) and StI (f_y=220MPa) are utilized for the reinforced bars. Steel class StI is used for the reinforcement of all beams (longitudinal and transverse) and for most column elements. In Figure 2a and 2b, it can be seen for which cases StIII is utilized. It should be noted that the provided concrete and steel strength material properties are defined following the German Institute for Standardization (DIN) standards (DIN 1045 [36] and 488 [37] for concrete and steel respectively). One important aspect is the fact that the two building units do not have common foundation. The foundation system of UNIT 1 consists of simple footings whereas in UNIT 2 the footings are partially combined with a raft foundation. Table 1 summarizes the main characteristics of the two building units according to the design and construction plans, namely the mass and the strength of concrete (f_c) and reinforcement steel (f_y). Mass values have been deduced from the available blueprints based on the structural elements and the prescriptions of the national loading standards. Regarding the non-structural components, besides the three existing elevators, an electricity generator is also installed in the basement of UNIT 1, which in case of a general shut down (e.g. due to a strong earthquake event) constitutes the only source of electricity supply for the entire hospital. Finally it should be noted that no significant interventions or retrofitting works have been carried out over the years according to the Technical service of the hospital that would allow deviations from the available design and construction plans.

Permanent and temporary instrumentation arrays have been implemented under the responsibility of the Soil Dynamics and Geotechnical Earthquake Engineering of the Aristotle University of Thessaloniki (SDGEE-AUTH) and in close cooperation with Helmholtz Centre Potsdam, German Centre for Geosciences (GFZ). The permanent network (SOSEWIN network) was installed for the long term building monitoring and for rapid assessment of damages. It is composed by sensing units where the building motion is measured in real time through MEMS sensors. It is mainly intended to monitor the building response to

earthquakes. Ambient noise measurements were used for the dynamic characterization of the building deploying a denser temporary network of stations equipped with velocimeters, which have a better amplitude resolution and a lower internal noise than the MEMS. The description of both permanent and temporary network provides a complete view of the instrumentation arrays that have been installed in the hospital building. The SOSEWIN accelerometric network operates on a continuous basis in AHEPA since May 2012 [33] and constitutes of 13 triaxial accelerometers (MEMS ADXL203 chip). In addition to the SOSEWIN network, various temporary seismometer arrays have been also deployed inside the hospital in the frame of the general risk assessment studies. In February 2013, ambient noise measurements were collected deploying a temporary array of 39 triaxial seismometers (Mark Products L4C-3D of 1Hz coupled to EarthData Logger, PR6-24, 24 bit digitizers) in the two building units. The seismic sensors are passive seismic sensors with 1Hz corner frequency, connected to 24bit digitizers. Even in the free field, the internal noise of such equipment allow to record ambient noise to about 0.2 Hz (e.g. [38]; [39]). Each floor of the building was instrumented with four seismometers in order to ensure the observability of translational and torsional modes. Fig. 1b reports the location of the seismometers installed along the middle corridor near and far from the structural joint. North direction of the stations was placed parallel to the longitudinal structural direction of the building. The sensors recorded along the two orthogonal horizontal and along the vertical directions (three components). The two horizontal components are oriented along the longitudinal and transversal direction of the building. Ambient noise was recorded by all stations simultaneously for about 4 hours in all stations with a sampling rate of 500 Hz and gain 10. The time synchronization among the stations was established through GPS antennas.

Table 1. Main characteristics of the hospital building units (f_c and f_y represent the strength of concrete and reinforcement steel respectively).

RC building	Total mass (t)	f_c (MPa)	f_y (MPa)
UNIT 1	3804.0	14.0	220.0 and 500.0
UNIT 2	3144.0	14.0	220.0 and 500.0

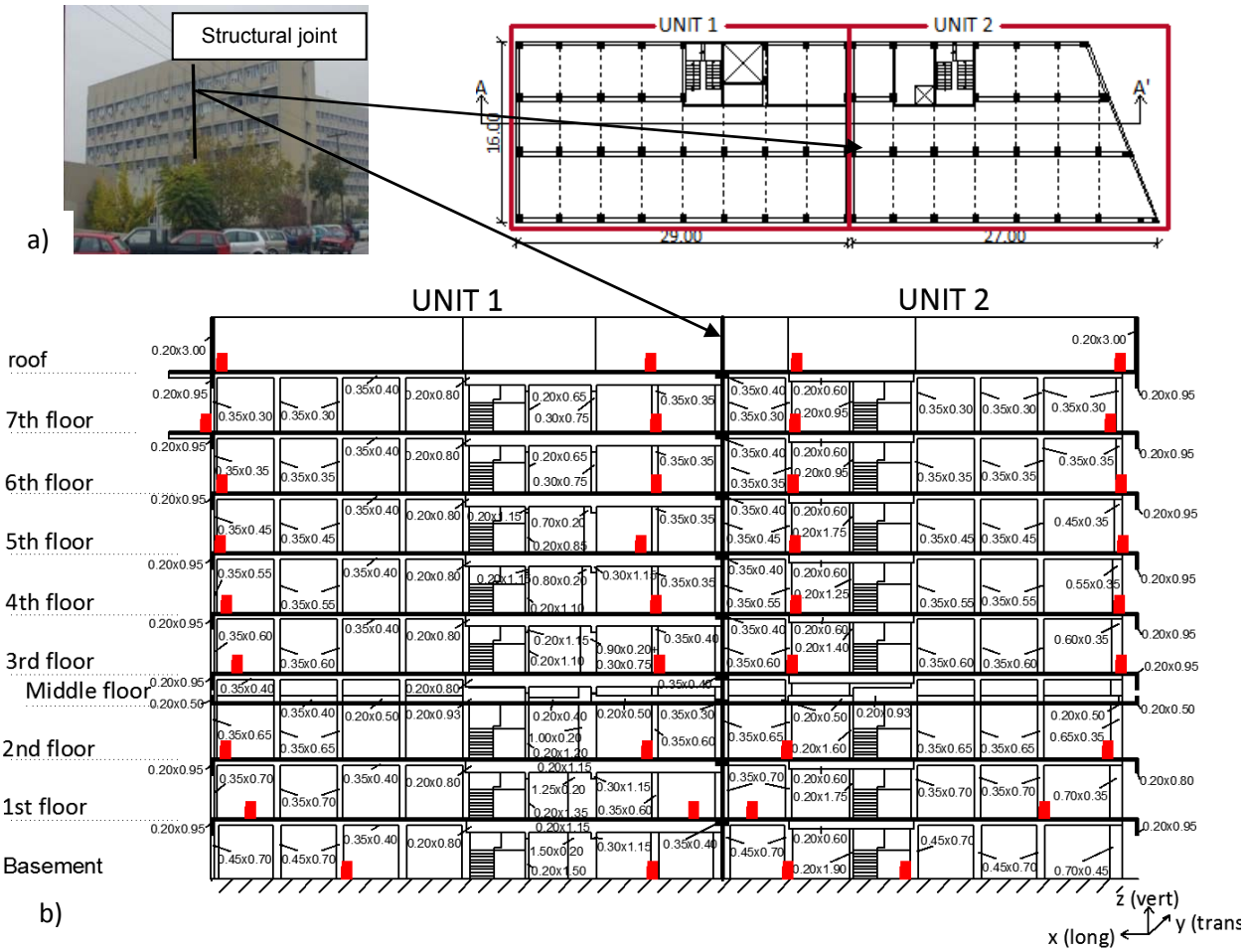

Fig.1. a) AHEPA hospital building and typical floor plan with the structural joint. b) Section A-A' along the longitudinal direction of the hospital building with the temporary instrumentation (red squares).

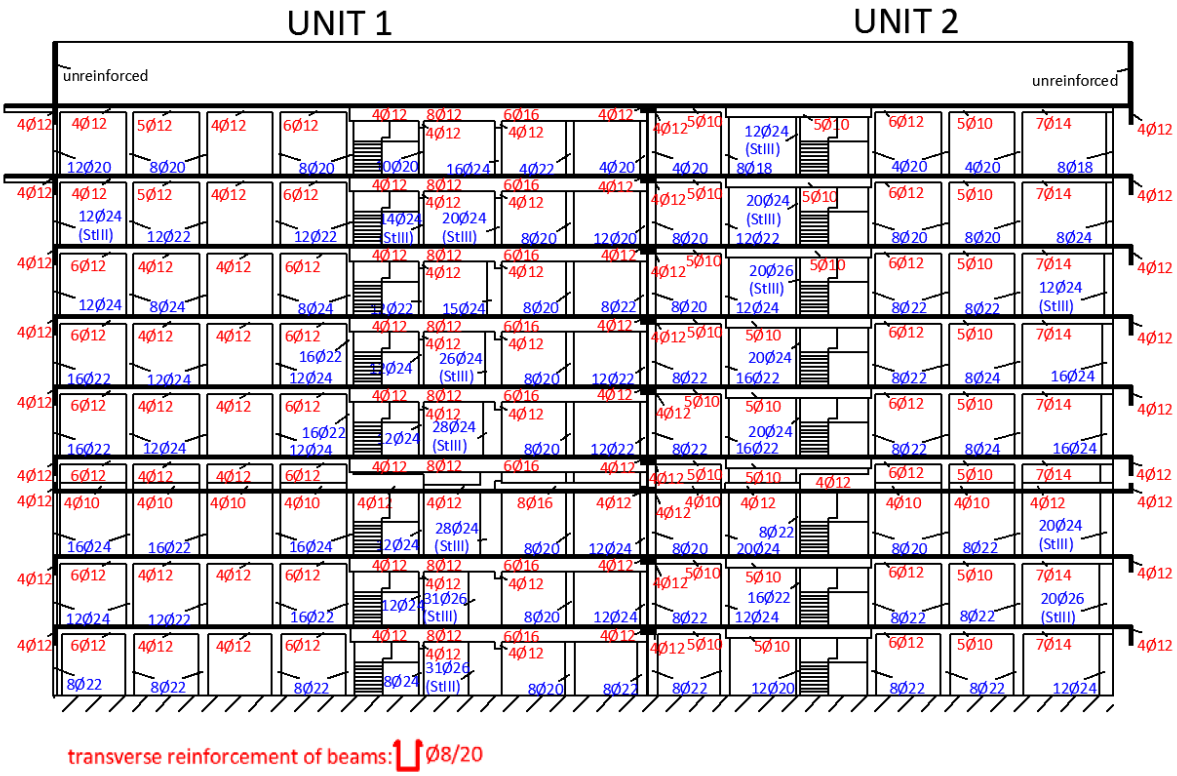

a)

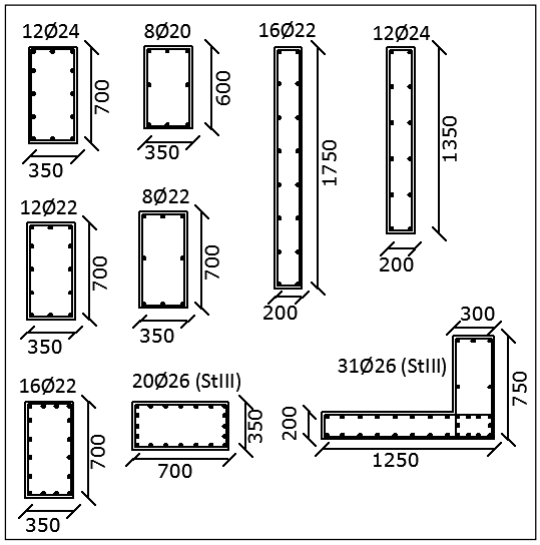

b)

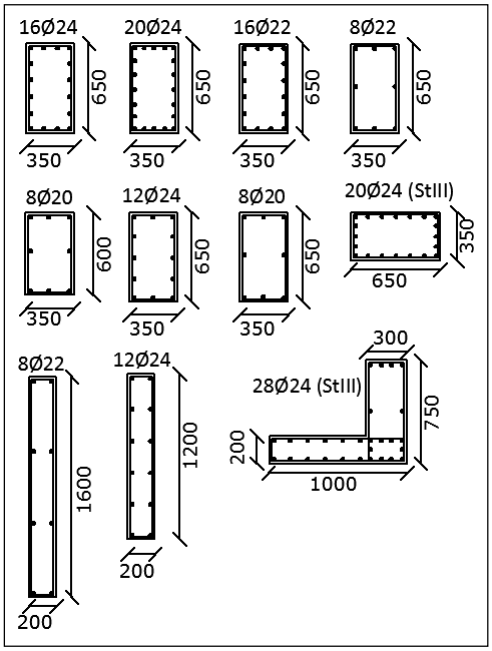

c)

Fig.2. a). Reinforcement layout of UNIT 1 and UNIT 2: red and blue correspond to the beam and column reinforcement respectively. b). Diameters and position of the column reinforced bars of the 1st and c) 2nd floors respectively (diameters and dimensions in mm),

252

253

3.”TIME-BUILDING SPECIFIC” VULNERABILITY ASSESSMENT OF THE HOSPITAL BUILDING UNITS USING MONITORING DATA

3.1. Description of the methodological framework

A schematic flowchart of the proposed methodological framework that has been adopted in the present study for the derivation of the ”time-building specific” fragility curves of the hospital building units based on field monitoring data is presented in Fig. 3. Ambient noise measurements are used to derive the experimental modal model of the hospital building and identify its modal properties based on operational modal analysis (OMA). The modal identification results are used to update and better constrain the initial finite element model of the building, which is based on the design and construction documentation plans. In the absence of any structural geometry modification since 1971 when the building was constructed, only the variation in the material properties is taken into account in the present study. An eigenvalue sensitivity analysis of the elastic numerical modal models is performed to identify the most sensitive parameters influencing the structural modes of interest which are used in the manual updating process to define the optimal analytical models that reflect the experimental results. The selection of the best updated finite element (FE) model for the two building units is made by evaluating an appropriate response correlation function between experimental and numerical results. Three-dimensional incremental dynamic analyses (IDA) [40] of the nonlinear updated models are performed using real ground motion accelerograms that are selected based on the regional seismic hazard, to derive the “time-building specific” fragility curves that correspond to the actual state of the hospital building units.

3.2 Operational modal analysis

To evaluate the dynamic characteristics of the hospital building, namely the natural frequencies and mode shapes, system identification and operational modal analysis are performed using MACEC 3.2 software [41] for the two adjacent building units separately (UNIT 1 and UNIT 2) as well as for the entire hospital building, analyzed as one, taking into account the interaction of the two building units due to their connection with the structural joint (namely BUILDING).

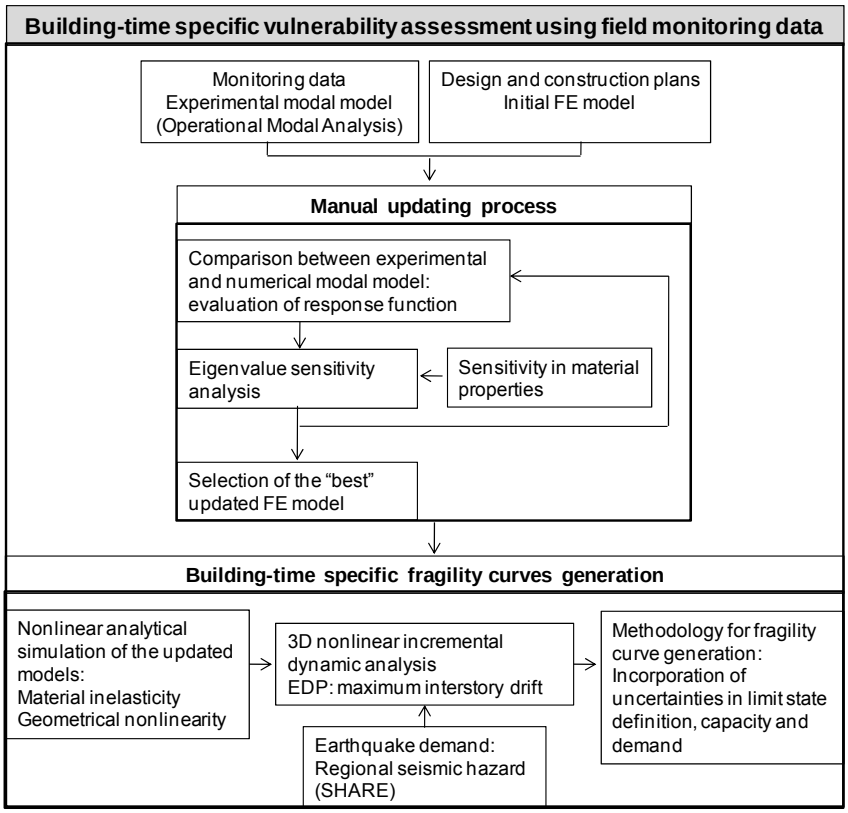

Fig.3. Methodological framework adopted in the present study.

In Bindi et al. [33], the modal parameters (frequencies, mode shapes) of the analyzed systems are extracted based on non-parametric identification techniques (Peak Picking-PP and Frequency domain decomposition-FDD). In the present paper modal analysis of the structural systems under study is conducted using parametric identification techniques, namely the Stochastic Subspace Identification-SSI [42] to verify and enhance the reliability of the non-parametric identification results.

Only the horizontal components (longitudinal and transverse) of the ambient noise recorded at the EDL seismometers of the 2013 temporary network (Fig. 1b) are used to perform system identification and operational modal analysis. The noise data are baseline corrected, filtered between frequencies 0.8 and 20 Hz and synchronized between all stations. A 10% cosine-taper is applied and the instrument response is removed from the records. A total duration of 1800 sec (30min) is used for OMA as tests for stability of the results in terms of modal parameter variation showed that 30 minutes are enough to get reliable results validated by means of appropriate techniques [43]. The grid of the models is built so that the defined nodes correspond to nodes that have been actually measured. The stations that are used for the identification process are illustrated in Fig. 1b.

The SSI technique involves the selection of a mathematical space-state model where the parameters are adjusted to the model so that it fits to the measured data. The goal of this model calibration is to minimize the deviation between the predicted and measured system

response. The number of the parameters of the linear, time invariant state space model, plays a significant role in the identification process; for example when a too small number is defined, the modal parameters may be not modeled statistically correctly. On the other hand, if the number is too high, then the model becomes over-specified resulting in unnecessary high statistical uncertainties of the model parameters. In general the selection of the model order for the construction of the stabilization diagrams for the SSI method depends on the number of modes of interest as well as the number of sensors. For the construction of the stabilization diagrams a model order range from 2 to 150 in steps of 2 was selected for UNIT 1 and UNIT 2, whereas for BUILDING the upper limit of the model order was increased to 200. The increase of the model order for BUILDING was required due to the analysis of a much larger data set as, data from 36 stations were used for the identification analysis in contrast to UNIT 1 and UNIT 2 where data from only 18 sensors were used. The results of the SSI analyses, namely the stabilization diagrams, for the two adjacent building units analyzed separately (UNIT 1 and UNIT 2) and as one single building (BUILDING) are presented in Fig. 4. The aim is to use these diagrams to detect the columns of stable modes that satisfy the defined stabilization criteria and continuously select a representative mode from each column.

Table 2 summarizes the five eigenfrequencies computed with both parametric (Fig. 4) and non-parametric system identification methods [33]. It should be noted herein that potential effects of the non-structural components did not influence the identification results. The electricity elevator was not operating during the experiment while other non structural elements, such as elevators and medical devices, are operating in high frequencies (f>10Hz) and are not affecting thus the frequency range of interest (f<10Hz). Comparing the results between the two techniques, it is observed that the estimated frequency values for the five well separated modes are very close to each other (practically the same for the first three modes) for the two identification methods applied as well as for the different system models identified.

Similar orders and shape types of the modes are estimated for the different system models (UNIT 1, UNIT2 and BUILDING) implying that the dynamic characteristics of the complex hospital building are possible to be captured by monitoring and analyzing the two adjacent building units separately. The mode shapes corresponding to the identified modes are presented in Fig. 5, 6 and 7. The building is exhibiting coupled sway and torsional modes in the frequency range of interest, which are expected in case of geometric and structural irregularities or eccentricities between the center of mass and center of rigidity. The highly coupled obtained mode shapes confirm the complex vibrational characteristics of the building especially for the first two identified frequencies. The resonant frequencies of the two adjacent units are very close which may be attributed to their similar mass and stiffness

properties. In order to gain insight of the modal behavior of the two units and to investigate the correlation between their mode shapes, the modal assurance criterion [44] for the identified modes is quantified as:

$$MAC_{ij} = \frac{\left(\varphi_j^T \varphi_{Ei}\right)}{\left(\varphi_j^T \varphi_i\right)\left(\varphi_{Ej}^T \varphi_{Ei}\right)} \quad (1)$$

where φ_j is the eigenvector j from the experimental modal model of UNIT 1 and φ_{Ei} the eigenvector i from the experimental modal model of UNIT 2. MAC values are calculated higher than 0.8 for the first, third and the fourth modes, approximately equal to 0.60 for the fifth mode while for the second mode MAC value is found to be lower than 0.60. Based on the MAC results, it is seen that mode shapes for the two building units are identical for the first, third and fourth modes. For the third and fifth modes which correspond to the same frequencies for both units, the mode shapes are not identical for the UNIT 1 and UNIT 2 although being of similar type. This may be attributed to the different geometrical and structural configurations of the two units. An interesting aspect is also the fact that mode 3 is identified for both units as torsional, however the mode shapes for the two structures are out of phase. Based on the above considerations the two units can not be considered as an entire monolithic building neglecting the influence of the structural joint as they do not present a common modal behavior. In fact the identified mode shapes reveal a coupling of the two building units under low vibration (operational conditions). The first and second mode shapes are identified as coupled translational modes mainly in the transverse direction. The difference between the two first modes is the fact that for both units the torsional component in the second mode shape is much more pronounced in comparison to the first one. Under no interaction, the second mode shape would be expected to be a coupled translational mode mainly in the longitudinal direction. Under strong ground motion however, due to the strong nonlinearities which the systems are expected to experience and taking into account the fact that the two units do not have common foundation, the interaction between the two units may be completely different affecting consequently their seismic response. For the above reasons the seismic vulnerability assessment is performed considering the two units separately. The aim of the updating procedure presented continuously is to calibrate the numerical models in order to reflect the elastic modal behavior of the two separate structural units as identified through the analysis of the noise measurements. The damping values extracted from the SSI analysis and reported in Table 2, appear to be consistent with the level of vibration for the first and second modes. On the other hand high damping estimates are extracted for the third, fourth and sixth modes, ranging approximately between 3-6%,

indicating that biases may probably have affected the obtained estimates for the higher modes as the latter do not reflect the ranges under operational conditions generally reported in seismic design and wind engineering manuals ([45]; [46]; [47]; [48]). Finally it should be noted that damping is not considered in the implemented updating formula.

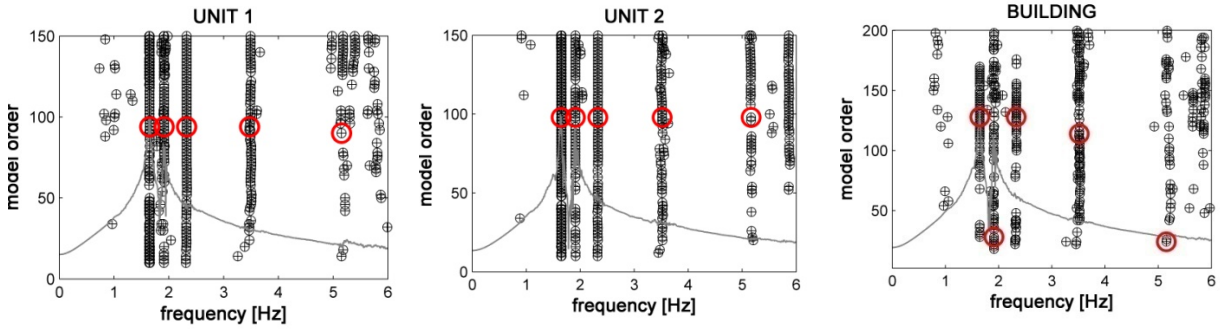

Fig.4. Modal identification using the Stochastic Subspace Identification (SSI) method using ambient noise measurements.

Table 2. Modal identification results for UNIT 1, UNIT 2 and BUILDING estimated using non-parametric FDD [25] and parametric SSI (present study) identification techniques.

Mode	Mode type	UNIT 1			UNIT 2			BUILDING		
		FDD (Hz)	SSI (Hz, ξ %)		FDD (Hz)	SSI (Hz, ξ %)		FDD (Hz)	SSI (Hz, ξ %)	
1	Coupled translational	1.65	1.65	0.8	1.65	1.65	0.9	1.65	1.65	0.8
2	Coupled translational	1.90	1.91	1.3	1.91	1.91	1.1	1.91	1.91	0.8
3	Torsional	2.33	2.33	3.6	2.35	2.33	3.5	2.35	2.33	3.2
4	1st longitudinal	3.50	3.47	5.4	3.58	3.52	5.8	3.58	3.51	6.4
5	2nd longitudinal	5.20	5.15	3.0	5.22	5.16	1.1	5.20	5.15	2.1

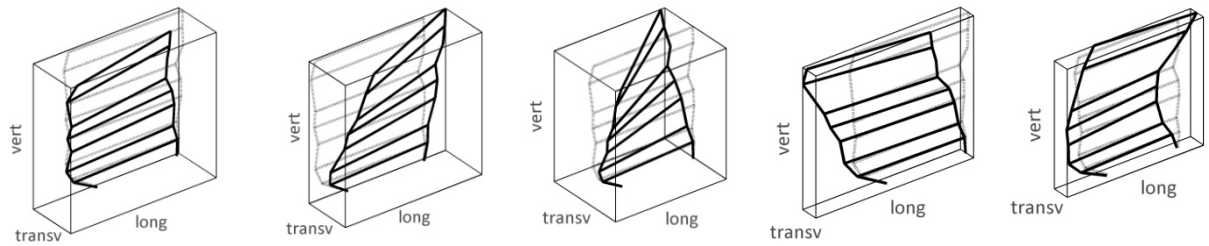

T_1=0.61sec f_1=1.65Hz | T_2=0.52sec f_2=1.91Hz | T_3=0.43sec f_3=2.33Hz | T_4=0.29sec f_4=3.47Hz | T_5=0.19sec f_5=5.15Hz

Fig.5. Mode shapes corresponding to the five first indetified frequencies for UNIT 1.

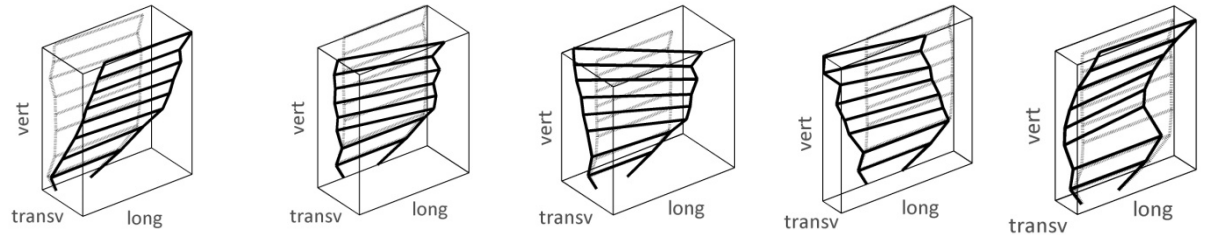

T_1=0.61sec f_1=1.65Hz | T_2=0.52sec f_2=1.91Hz | T_3=0.43sec f_3=2.33Hz | T_4=0.28sec f_4=3.52Hz | T_5=0.19sec f_5=5.16Hz

Fig. 6. Mode shapes corresponding to the five first indetified frequencies for UNIT 2.

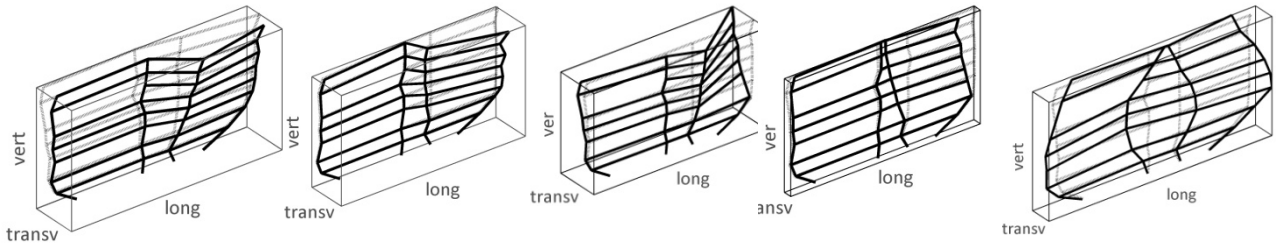

T_1=0.61sec f_1=1.65Hz | T_2=0.52sec f_2=1.91Hz | T_3=0.43sec f_3=2.35Hz | T_4=0.28sec f_4=3.51Hz | T_5=0.19sec f_5=5.15Hz

Fig. 7. Mode shapes corresponding to the five first indetified frequencies for BUILDING.

3.3 Finite element model updating

Model updating aims at the “correction” or “update” of the initial finite element model based on data processing, obtained from measurements conducted on the test structure [49]. The main purpose is to modify iteratively updating parameters to result in structural models that better reflect the measured data than the initial ones. One of the key issues during the updating process is the selection of the appropriate updating parameter. In general, if not serious geometrical modifications are identified, as in the present test case, structural features, such as material or mass properties, are likely to be selected as updating parameters in order to increase the correlation between the observed dynamic response of the structure and the predicted from the numerical modal model [50]. Other parameters such as soil-structure interaction, condition and aging of the foundations after a strong earthquake, the connection between structural elements which influence the modal properties, may contribute in the updating process, however include high uncertainty levels and additional tests may be required for their determination (e.g. non-destructive tests). For the AHEPA case study, soil-structure interaction effects are not expected to be pronounced as the soil is characterized as stiff clay with an average shear wave velocity over the upper 30-35m equal to 450m/s [33]. Besides, for the extracted modes (particularly for the three first modes) that are used in the updating procedure, the modal displacements extracted from the ambient vibration measurements corresponding to the basement nodes are much smaller in comparison to the top floor nodes for both buildings allowing the fixed base assumption. On the other hand the evaluation of the condition and aging of the foundations after the Thessaloniki earthquake or the quality of the connections between structural elements is not indicated as limited information is provided by the blueprints and data from non-destructive tests are not available. The aim of the updating procedure in the present study is to conduct an extensive parametric study of the hospital buildings considering the variation in structural parameters (e.g. modulus of elasticity), in order to investigate the sensitivity of the model to

material properties, and how the latter may affect the overall stiffness of the structure. A manual updating scheme is applied considering only a limited number of parameters, which however allows a good observation of the process in order to gain complete insight on the effects of the sensitivity parameters on the structural behavior. The initial numerical modal model of the buildings under study is based on the design and construction documentation plans. The numerical modeling is conducted for the two adjacent units separately using OpenSees finite element platform [51]. Elastic beam-column and truss elements are employed to model the linear RC elements (beams and columns) and masonry infills respectively. For the linear modeling of the masonry infills a double strut model is adopted to represent the in-plane behavior of the infill panel. Fixed base conditions are assumed for both structural models.

The updating procedure is performed not only to improve the frequencies of the considered modes of the initial numerical model presented in Tables 3 and 4, but also to calibrate the numerical mode shapes in order to fit the experimental data. Only the third mode of the numerical modal model was identical to the respective experimental one for both units. On the other hand the mode shapes of the first and second modes needed to be updated in order to capture the coupled sway modes reflecting thus the experimental results preserving at the same time the torsional mode shape of the third mode. As sensitivity parameter for the updating procedure, the compressive strength of the masonry infill, f_m, is selected to take into account the uncertainties of the material behavior as well as the possible heterogeneity between the material properties of the different infill parts. Besides the masonry strength of the infills, also the sensitivity in the concrete strength was investigated as well as the combination of both parameters. The updating procedure using the concrete strength showed that frequencies and mode shapes are not affected significantly. Thus only one sensitivity parameter is used, namely the compressive strength of the infill panels, in order to avoid complicated updating schemes and allow a better observation of the updating procedure. A suite of numerical modal models is generated assuming a normal distribution for f_m and defining possible scenarios adopting different infill masonry compressive strength values and configurations [50]. The random properties of the masonry compressive strength, namely the mean value μ=3MPa and its covariance COV=20% are defined according to Mosalam et al. [52]. For the initial finite element model the compressive masonry strength is considered equal to the mean value μ=3MPa. The different values of compressive strength for the considered updating scenarios are subsequently computed based on the mean and standard deviation σ according to the adopted normal distribution considering a limit range for the mean value of μ-3$\sigma \leq f_m \leq \mu$+3σ. Then the elastic modulus in compression, E_m, which is used as input parameter to simulate

the masonry infills, is estimated based on the adopted mean value for the compressive strength according to the relation E_m= 1000f_m [53].

To take into account the heterogeneity of the masonry mechanical properties as well as the possible variation between the material properties and the modulus of elasticity of the different parts, several updating scenarios are investigated. In particular five different scenarios are defined based on the variation in f_m (or E_m) and the considered configurations of the masonry infills for the selection of the best model as illustrated in Fig. 8.

- Scenario 1: single value of elastic modulus for all the perimeter of the two buildings E_m
- Scenario 2: different values of elastic modulus for (a) the longitudinal E_{mlong} and (b) the transverse $E_{mtransv}$ infills
- Scenario 3: different values of elastic modulus for (a) the longitudinal infills depending their location E_{mlong1} and E_{mlong2}, (b) the transverse infills far from the joint $E_{mtransv1}$ and (c) the transverse infills close to the joint $E_{mtransv2}$
- Scenario 4: different values of elastic modulus for (a) the longitudinal and (b) the transverse infills building by building (UNIT1: E_{mlong1}, $E_{mtransv1}$ / UNIT2: E_{mlong2}, $E_{mtransv2}$).
- Scenario 5: different values of elastic modulus for all infills along the perimeter regardless their location (E_{mlong1}, E_{mlong2}, E_{mlong3}, E_{mlong4}, $E_{mtransv1}$, $E_{mtransv2}$, $E_{mtransv3}$, $E_{mtransv4}$).

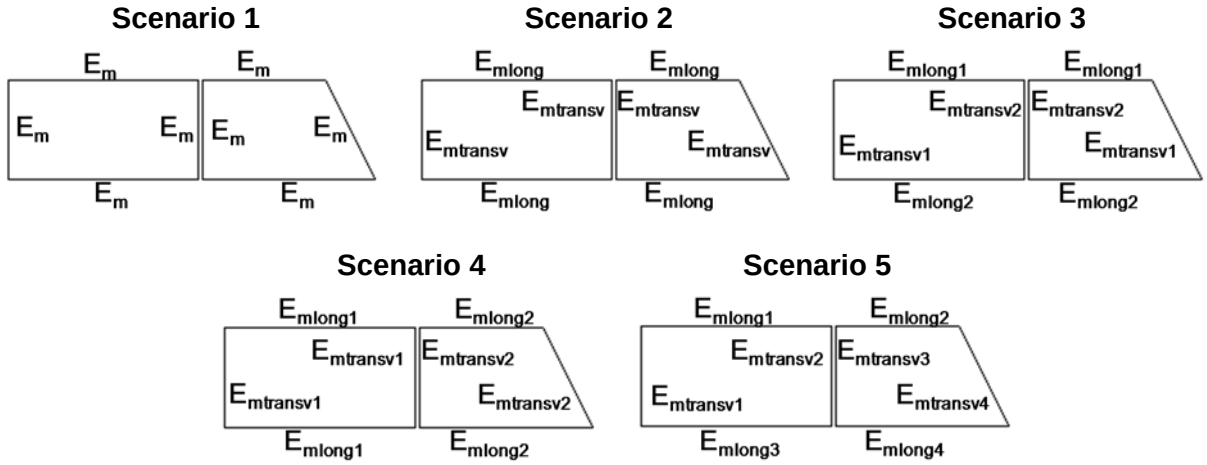

Fig.8. The different updating scenarios adopted within this study.

Modal analyses for all the derived numerical modal models are performed in OpenSees for the three dimensional elastic linear finite element models of the two adjacent buildings separately (UNIT 1 and UNIT 2). Only one among them is considered as the best model representing the measured dynamic response. The selection of the best model is based on the evaluation of the Modal Assurance Criterion-MAC [44] defined according to Equation 1 where φ_j is the eigenvector j from numerical modal model and φ_{Ei} the eigenvector i from field monitoring test. The computation of the MAC values and the correlation of the responses

between the experimental and numerical modal models are made at 18 nodes for each building unit (2 nodes per floor at each unit corresponding to the sensor locations). A good correlation between the two tested modes is considered to be achieved for MAC values greater than 0.8. The scenario that represents most accurately the experimental results for the modes under investigation is found to be the one corresponding to the updating scenario 3. The elastic moduli in compression of masonry infills adopted for this scenario were the following: E_{mlong1}= 3GPa (f_m=μ=3MPa), E_{mlong2}=1.8GPa (f_m=μ-2σ=1.8MPa), $E_{mtransv1}$=3GPa (f_m=μ=3MPa) and $E_{mtransv2}$=4.8GPa (f_m=μ+3σ=4.8MPa).

Due to the complexity of the structure under study only the first three modes are considered in the updating process, which represent the fundamental deformation modes of the structure and activate approximately 80% of the total mass of the building units. In Tables 3 and 4 the results of the updating methodology for UNIT 1 and UNIT 2 are presented respectively. The eigenfrequencies and mode shapes of the updated finite element models are compared to the initial ones as well as to the experimental results. It is seen that for UNIT 1, the updated finite element model correlates well with the experimental results for all the modes under investigation (MAC>0.8). For UNIT 2 on the other hand, MAC values are high for the 1st and 3rd mode, indicating the satisfactory correlation between analytically and experimentally calculated modal parameters, whereas for the 2nd mode it was not possible to achieve MAC values greater than 0.8. This may be attributed to the fact that the structural configuration of UNIT 2 (trapezoidal plan section) did not allow to capture the 2nd mode shape and probably another sensitivity parameter related not only to the structural stiffness (such as the masonry compressive strength) but also to the storey mass or a combination of several parameters related to both stiffness and mass, would be more appropriate. Given however the difficulties in proper asserting the mass properties of the complex hospital building (e.g. distribution of mass along height and floor), this parameter is not used in the updating procedure as the associated uncertainties may reduce the accuracy of the results.

Table 3. Comparison of the updated finite element model of UNIT 1 with the initial model and the experimental results (T: period, f: frequency).

Initial FEM T (sec)/f(Hz)	Mode shape of updated FEM T (sec)/f(Hz)	Mode shape of experimental model T(sec)/f(Hz)	MAC
Coupled translational T_1=0.69sec/f_1=1.46Hz	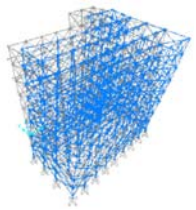	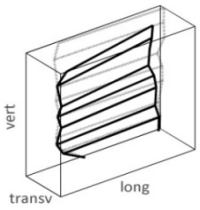	0.96
	T_1=0.64sec/f_1=1.56Hz	T_1=0.61sec/f_1=1.65Hz	
Coupled translational T_2=0.48sec/f_2=2.06Hz	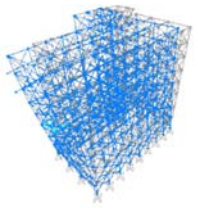	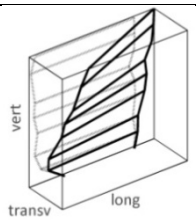	0.94
	T_2=0.53sec/f_2=1.89Hz	T_2=0.52sec/f_2=1.91Hz	
Torsional T_3=0.37sec/f_3=2.70Hz	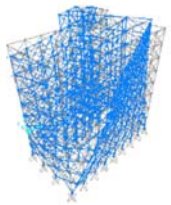	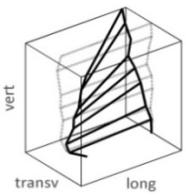	0.97
	T_3=0.37sec/f_3=2.70Hz	T_3=0.43sec/f_3=2.33Hz	

Table 4. Comparison of the updated finite element model of UNIT 2 with the initial model and the experimental results.

Initial FEM T (sec)/f(Hz)	Mode shape of updated FEM T (sec)/f(Hz)	Mode shape of experimental model T(sec)/f(Hz)	MAC
Coupled translational T_1=0.67sec/f_1=1.50Hz	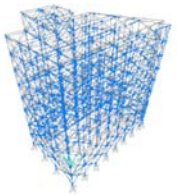	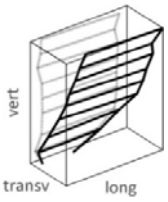	0.98
	T_1=0.65sec/f_1=1.54Hz	T_1=0.61sec/f_1=1.65Hz	
Coupled translational T_2=0.49sec/f_2=2.05Hz	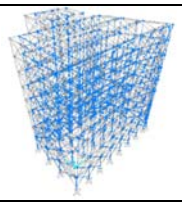	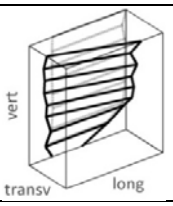	0.45
	T_2=0.53sec/f_2=1.89Hz	T_2=0.52sec/f_2=1.91Hz	
Torsional T_3=0.36sec/f_3=2.77Hz	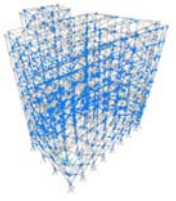	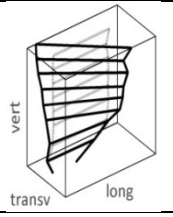	0.94
	T_3=0.35sec/f_3=2.86Hz	T_3=0.43sec/f_3=2.33Hz	

3.4 Nonlinear finite element modeling

The nonlinear numerical modeling of the structure is conducted using OpenSees finite element platform [51]. Inelastic force-based formulations are employed for the simulation of the nonlinear three-dimensional, with six degrees of freedom, beam-column frame elements. The applied formulations allow both geometric and material nonlinearities to be captured. Distributed material plasticity along the element length is considered based on the fiber approach to represent the cross-sectional behavior. Each fiber is associated with a uniaxial stress-strain relationship; the sectional stress-strain state of the beam-column elements is obtained through the integration of the nonlinear uniaxial stress-strain response of the individual fibers in which the section is subdivided. For both initial and updated units, the material strength properties for concrete and steel summarized in Table 1 are used for the definition of the stress-strain relationship. The Popovics [54] concrete model is used to define the behavior of the concrete fibers. Due to the fact that the building units were designed according to low seismic code provisions with non sufficient transverse reinforcement, the element sections are considered to be unconfined. The uniaxial 'Concrete04' material is used to construct a uniaxial Popovics concrete material object with degraded linear unloading/reloading stiffness according to the work of Karsan and Jirsa [55] with zero tensile strength. The steel reinforcement is modeled using the uniaxial 'Steel01' material to represent a uniaxial bilinear steel material with kinematic hardening described by a nonlinear evolution equation. For the nonlinear modeling of the masonry infills inelastic struts are used to represent infill walls as they provide sufficient accuracy to capture key characteristics of the force-displacement response. The nonlinear behavior of the infill panels is reflected by assigned axial load hinges on the diagonal struts whose characteristics are determined as given in FEMA-356 [56]. Each strut is assigned an elasto-plastic force displacement relationship representing initial stiffness and peak strength behavior of the masonry. The infill material strength for the initial models is taken equal to the mean value adopted for the updating procedure (μ=3 MPa) while for the updated models the masonry strength is defined based on the selected updated scenario described in Section 3.3. The structural models do not include any contribution from non-structural components or from gravity-load resisting structural elements that are not part of the lateral resisting system. Since non-destructive tests were not possible to be conducted and details for the formation of the beam-column joints were not available from the blueprints, rigid connection is considered for the modeling of the joints between beam and column. To take into account the rigidity against the in-plane deformation of the floor slabs, diaphragm constraint is employed. For both structural models fixed base conditions are assumed.

3.5 Selection of the input motion

A representative set of accelerograms is selected to perform the non-linear incremental dynamic analysis. The selected earthquake scenario consists of a set of 15 real ground motion records (Table 5) obtained from the European Strong-Motion Database (http://www.isesd.hi.is). They are all referring to stiff soil conditions classified as soil type B according to EC8 [57] with moment magnitude (M_w) and epicentral distance (R) that range between $5.8<M_w<7.2$ and $0<R<45$km respectively. Soil type B is the soil category of the foundation soil according to a detailed geotechnical survey performed in the site [58]. In order to eliminate potential source of bias in structural response, the selection of pulse-like records is avoided. The primary selection criterion was the average acceleration spectra of the set to be of minimal "epsilon" [59] at the period range of $0<T<2$sec with respect to the regional acceleration spectrum adopted from SHARE for a 475 year return period (http://portal.share-eu.org:8080/jetspeed/portal/). The optimization procedure was performed making use of the REXEL software [60]. The mean normalized elastic response spectrum of the records is illustrated in Fig. 9 in comparison with the corresponding reference spectrum adopted from SHARE. A good fit between the two spectra is achieved.

Table 5. List of records used for the IDA.

Earthquake Name	Station ID	Date	M_w	R [km]	PGA_X [m/s^2]	PGA_Y [m/s^2]	Waveform ID
Friuli (aftershock)	ST28	15/9/1976	6.0	14	1.3841	2.3189	000147
Izmit (aftershock)	ST3265	13/9/1999	5.8	23	1.8983	1.2837	006959
Montenegro (aftershock)	ST76	24/5/1979	6.2	21	1.6273	1.3034	000231
South Iceland	ST2488	17/6/2000	6.5	17	3.9202	2.3852	004676
Kalamata	ST164	13/9/1986	5.9	10	2.1082	2.9095	000413
Izmir	ST162	6/11/1992	6.0	41	0.6527	0.8007	000549
Potenza	ST99	3/2/1998	5.8	36	0.7848	0.8544	000944
Ano Liosia	ST1101	7/9/1999	6.0	17	1.171	1.0661	001314
Tithorea	ST166	18/11/1992	5.9	25	0.3709	0.2744	000550
Ano Liosia	ST1258	7/9/1999	6.0	14	2.3842	2.1588	001714
South Aegean	ST1310	23/5/1994	6.1	45	0.5976	0.4023	001881
Ano Liosia	ST1255	7/9/1999	6.0	20	0.8549	0.7604	001711
Valnerina	ST83	19/9/1979	5.8	39	0.3855	0.2303	000244
Friuli (aftershock)	ST35	15/9/1976	6.0	21	4.6466	4.9562	000126
Duzce 1	ST3134	12/11/1999	7.2	11	1.0914	0.7137	006494

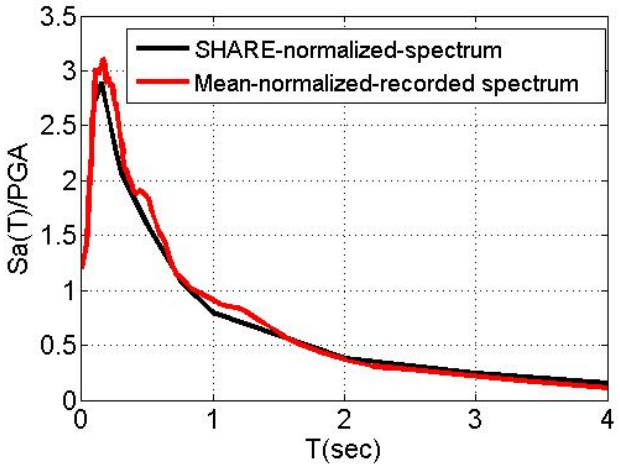

Fig.9. Normalized average elastic acceleration response spectrum of the input motions compared with the corresponding reference spectrum adopted from SHARE for a 475 year return period (http://portal.share-eu.org:8080/jetspeed/portal/).

571

572 *3.6 Incremental Dynamic Analysis*

573 The IDA procedure [40] is used to determine the seismic performance and assess the
574 seismic vulnerability of the initial and updated finite element models of UNIT 1 and UNIT 2.
575 Within this study the damage measure is expressed in terms of maximum inter-storey drift
576 ratio, which is generally used as engineering demand parameter in assessment studies of
577 frame buildings as it relates well to dynamic instability and structural damage [61]. More
578 specifically, the maximum peak SRSS drift, maxISD (i.e. the maximum over all stories of the
579 peak of the square-root-sum-of-squares of each storey's drift) in the two principal directions
580 is selected [62]. The seismic intensity is described using peak ground acceleration (PGA)
581 recorded on soil type B according to EC8 [57]. PGA is selected as intensity measure due to
582 the fact that the derived curves are incorporated in an operational tool for Early Earthquake
583 Warning and rapid post-event damage assessment that will be used by the civil protection
584 authority of the hospital. In this context, PGA is considered appropriate due to its simple
585 computation in real-time and its efficient use by the authorities.

586 IDA is conducted for the structural models by applying the 15 progressively scaled
587 records of Table 5. In particular, a PGA-stepping tracing algorithm is applied for each record
588 with an initial step of 0.1g, a step increment of 0.1g and a first elastic run at 0.05g. For
589 certain records it was necessary to reduce the step size of the algorithm to increase the
590 accuracy close to the flatline of the IDA curve. The minimum number of converging runs is
591 allowed to vary from 10 to 15 per record depending on the characteristics of the structure
592 and the record itself.

593 The fiber based approach that has been adopted for the nonlinear modeling of the
594 structures simulates sidesway collapse associated with strength and stiffness degradation

along the total length of beams and columns. The section and reinforcement details presented in Fig.2 reveal stronger columns – weaker beam formations. The analysis model does not directly capture column shear failure as the columns in this study are expected to yield first in flexure rather than experiencing direct shear failure, as in the case of squat non-ductile RC columns. It should be noted herein that results may change depending on the role of brittle failures. For the hospital building case however attention is focused only to a single aspect of the structural behavior since collapse modes for the particular building units are related to column flexural failures in the lower storeys ([63]) which are defined for each ground motion based on the intensity (peak ground acceleration) of the input ground motion that results in structural collapse, identified in the analysis by excessive interstorey drifts.

By interpolating the derived pairs of PGA and maxISD for each individual record 15 continuous IDA curves for each structural model are derived. Fig. 10b illustrates representative IDA curves for each record in terms of PGA for the updated finite element models of UNIT 1 and UNIT 2. For the purpose of the present study, two limit states are defined in terms of inter-storey drift ratio based on the IDA results, representing the immediate occupancy (IO) and collapse or near collapse prevention (CP) performance levels. The first limit state, namely the Immediate Occupancy corresponds to the yielding point where the elastic branch gives place to the post-elastic branch. The second limit state is assigned at a point where the IDA curve is softening towards the flat line, but at low enough values of maxISD so that we still trust the structural model [64]. Thus different IO and CP limit state values are chosen on the IDA curves for the same structure depending on the reference finite element model (initial or updated) and the individual record. For both initial and updated models of UNIT 1 and UNIT 2 the median of the first limit state is found equal to 0.1%, which is in line also with the proposed limit value of HAZUS for moment resisting infilled frame buildings. The median of the defined CP limit states in terms of SRSS inter-storey drift (maxISD) is used to define the CP limit state of the structure, which for both structures is found to be equal to 1.4% and 1.1% for the initial and updated models respectively. The assignments of the IO and CP limit state points on the IDA curves of the updated units are presented in Fig. 10a, 10b. The dispersion that is observed in the definition of the collapse prevention limit value may be attributed on one hand to the record-to-record variability in terms of frequency content and duration and on the other hand to the fact that PGA is used as intensity measure as in this case the seismic response and vulnerability depends on the input ground motion sets [65].

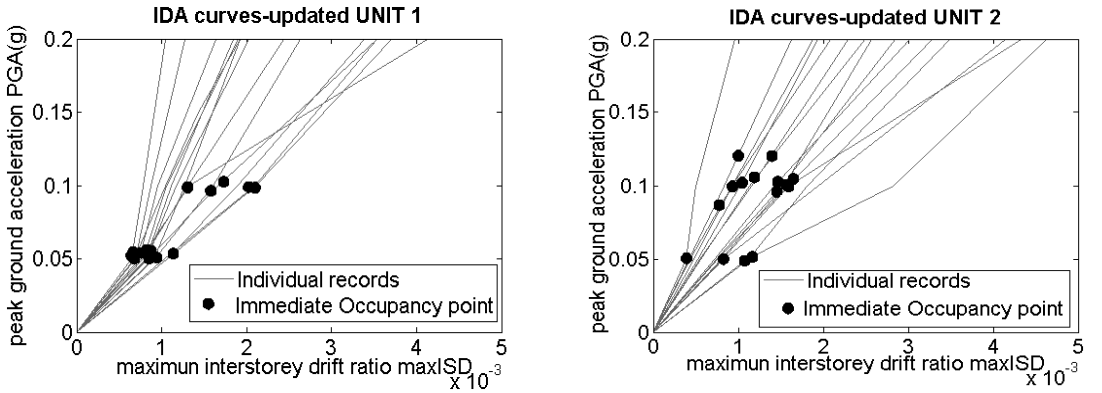

a).

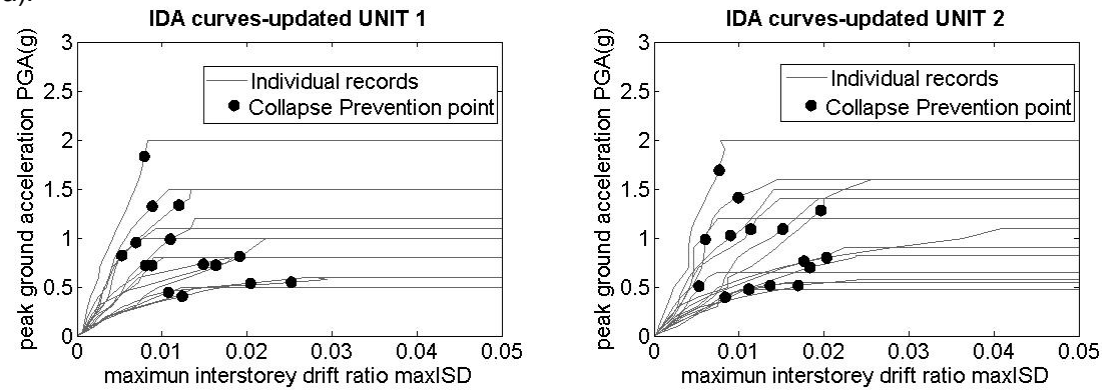

b).

Fig.10. Assignments of the immediate occupancy a): (IO) and b): collapse prevention (CP) limit damage state points on the IDA curves for the updated units.

3.7 Derivation of fragility curves

A fragility curve represents a graphical relationship of the probability of exceeding a predefined level of damage (e.g. IO, CP) under a seismic excitation of a given intensity. The results of the IDA (PGA - maxISD values) are used to derive the fragility curves for both analyzed buildings, expressed as a two-parameter lognormal distribution functions. Equation 2 represents the cumulative probability of exceeding a damage state *DS* conditioned on a measure of the seismic intensity *IM*.

$$P[DS / IM] = \Phi\left(\frac{ln(IM) - ln(\overline{IM})}{\beta}\right) \quad (2)$$

where Φ is the standard normal cumulative distribution function, *IM* is the intensity measure of the earthquake expressed in terms of PGA (in units of *g)*, $\overline{IM}$ and β are the median values (in units of *g)* and log-standard deviations respectively of the building fragilities and *DS* is the damage state. The median values of PGA corresponding to the prescribed performance levels are determined based on a regression analysis of the nonlinear IDA results (PGA-maxISD pairs) for both building units. More specifically a linear regression fit of the

643 logarithms of the PGA- maxISD data which minimizes the regression residuals is adopted in
644 the analysis cases. Fig. 11 presents the PGA - maxISD relationships for the updated models
645 of both UNIT 1 and UNIT 2, where it is noticed that the results show similar distribution and
646 curve fitting.
647 Three primary sources of uncertainties are generally taken into account for the
648 estimation of the total variability associated to each damage state for conventionally derived
649 fragility curves, namely the variability associated with the definition of the damage states, the
650 capacity of the structure and the seismic demand. Demand uncertainties are associated to
651 the effects of ground motion record-to-record variability on building response. Capacity
652 uncertainty reflects the variability of structural properties as well as the fact that the modeling
653 procedures are not perfect. Damage state definition uncertainties are due to the fact that the
654 thresholds of the damage indices or parameters used to define damage states are not known
655 [66]. In the present study the uncertainty associated with the demand is taken into
656 consideration by calculating the dispersion of the logarithms of PGA - maxISD simulated data
657 with respect to the regression fit. The log-standard deviation value in the capacity is assumed
658 to be 0.3 for the low code structures following the HAZUS prescriptions [67]. Uncertainties in
659 how well the nonlinear simulation model represents the behavior of the real building as well
660 as the highly nonlinear structural behavior near collapse are incorporated in the collapse
661 assessment and are reflected in the fragility curves through the consideration of the capacity
662 uncertainty. As far as the uncertainty in the definition of the damage states is concerned, the
663 damage limit values are defined on the IDA curves and since they are considered building
664 specific, the additional uncertainty related to the definition of the damage states is not taken
665 into consideration. Based on the above considerations, the definition of the limit state values
666 is implicitly related to the material properties and structural modeling and is therefore
667 incorporated in the uncertainty associated with the capacity. As discussed in [6] and [68] in-
668 situ tests and vibration measurements may improve the knowledge of the building's response
669 and its seismic behavior reducing thus the epistemic uncertainties associated with the
670 capacity. In the present study the use of ambient noise measurements to improve the
671 knowledge regarding the elastic behavior of the structure may reduce the epistemic
672 uncertainties for the IO limit state, however for the definition of the CP state, there are
673 significant underlying uncertainties which cannot be neglected as nonlinear behavior of
674 structures under strong motion introduces variations of the modal parameters and influences
675 their seismic response. Therefore the uncertainty in the capacity is not further reduced.
676 Under the assumption that the log-standard deviation components of demand and capacity
677 are statistically independent, the total log-standard deviation is estimated as the root of the
678 sum of the squares of the component dispersions. The herein computed log-standard

679 deviation β values of the curves vary from 0.6 to 0.68 for the considered finite element
680 models of the adjacent building units.
681 Fragility curves are derived for the initial and updated finite element models of UNIT 1
682 and UNIT 2. The initial as built numerical models are based on the available design plans
683 and correspond to the initial state of the structures ("building specific"), whereas the updated
684 models reflect the measured responses and therefore represent their actual state ("time-
685 building specific").
686 The calculated "building-specific" fragility curves of UNIT 1 and UNIT 2 that
687 correspond to their initial state are evaluated through their comparison with conventional
688 curves from the literature [3] that are derived for representative models of the same typology
689 (high-rise, regularly infilled, moment resisting frame structures designed with low seismic
690 provisions). More specifically, in Fig. 12 the derived curves are compared with the generic
691 curves proposed by Kappos et al. ([69] & [70]) for the specific typology. It is noted that most
692 of the work presented in Kappos et al. [70] was carried out by the same authors within the
693 framework of the RISK-UE project [69]. The differences between the results (given in terms
694 of fragility functions) of Kappos et al. [69] and [70] are probably due to slight geometric
695 differences adopted for the studied RC building typologies. A good match between the
696 curves is observed for the IO limit state as both generic curve sets are very close to the
697 calculated ones. However for the CP state it is seen that the "building-specific" curves
698 corresponding to the as-built state of the hospital case study are comparable only with the
699 curves of Kappos et al. [69] and differ significantly from the respective curves of Kappos et
700 al. [70], which is indicative of the non negligible variability that may be observed between
701 generic fragility curves.
702 The initial fragility curves are further validated through the computation of the
703 expected damage probability of the hospital building for the 1978 destructive earthquake in
704 Thessaloniki [71] as they are considered to better reflect the state of the structure at the time
705 of the event which occurred quite soon after their construction (in 1971). For a representative
706 intensity value for the specific seismic event equal to 0.3g the probabilities of slight damage
707 (IO state) and collapse (CP state) according to Fig. 12 are approximately estimated to 95-
708 98% and 2-3% respectively. These probabilities are consistent with the actual reports of that
709 time that no considerable earthquake damage was observed for the specific building.
710 In Fig. 13 the updated numerical models are compared with the initial ones for both
711 building units. The updated curves present a shift to the left in comparison to the initial ones,
712 indicating an increase in the structures' vulnerability which is more noticeable for the CP limit
713 state and for higher intensities. Since this difference in the fragility between the initial and
714 updated models is not attributed to geometrical modifications but to the variation and
715 distribution of material properties, it could be assumed that the increase in the building's

716 fragility is in fact an evidence of potential degradation of the structure over time. As no
717 significant damages have been reported for the specific building during past earthquake
718 events, the structural deterioration may be related to aging effects, which are further
719 analyzed in the following section.
720

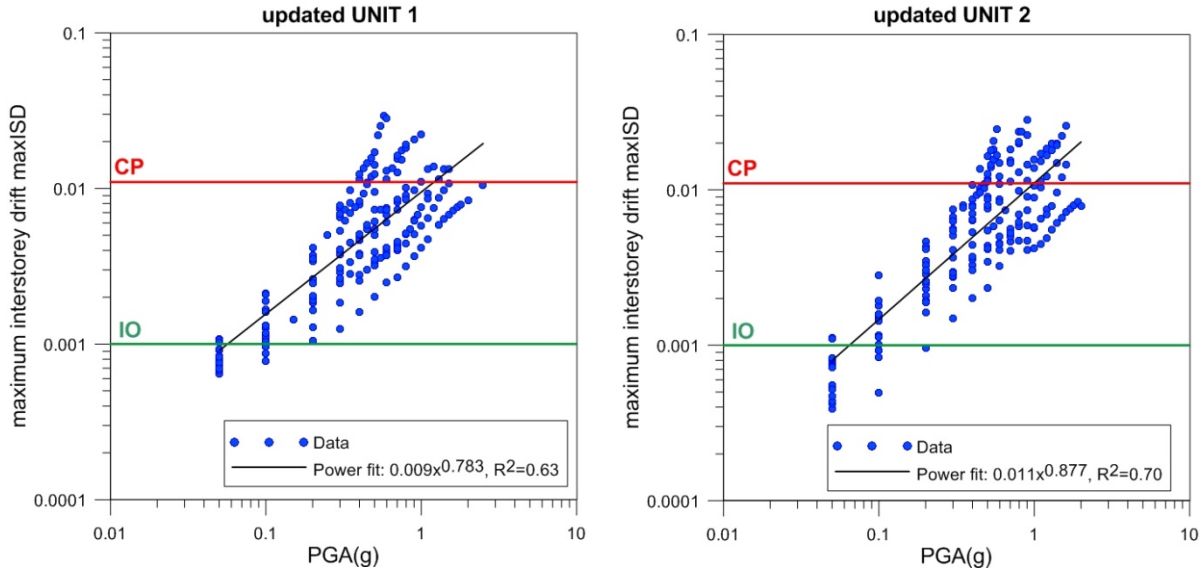

Fig.11. PGA-maxISD relationships for updated finite element models of UNIT 1 and UNIT 2.
721
722

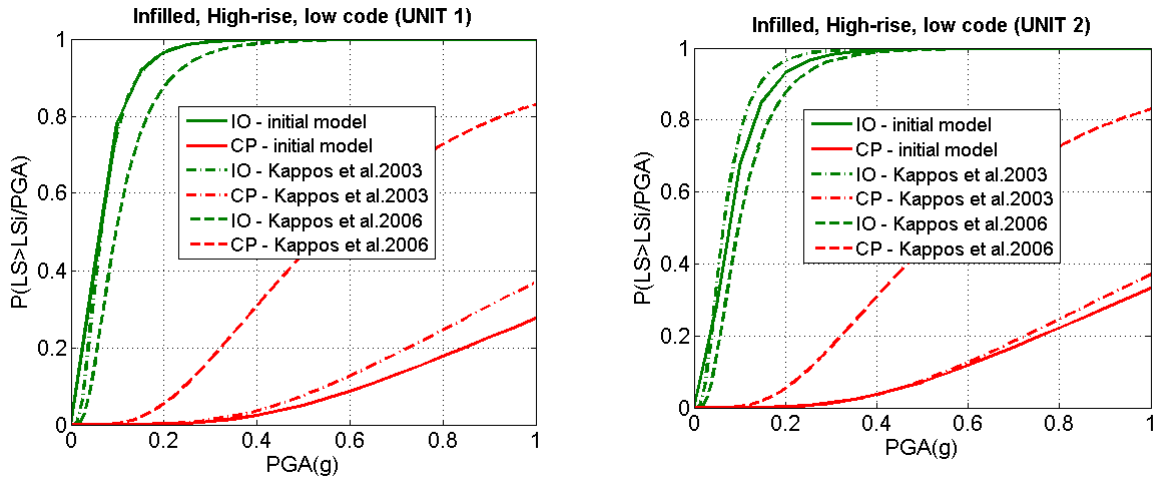

Fig.12. Comparative plots of the initial fragility curves derived for the two adjacent building units with the corresponding fragility curves provided by Kappos et al. ([69] & [70]).

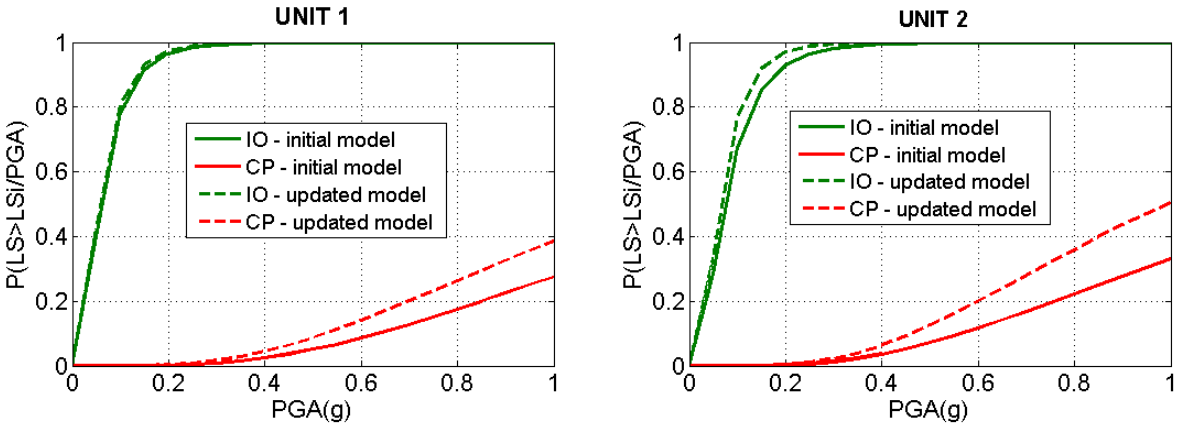

Fig.13. Comparative plot of the "building-specific" fragility curves derived for the initial and updated models of UNIT 1 and UNIT 2.

4. Comparison with the time-dependent fragility curves of the hospital building units

4.1 Deterioration modeling due to corrosion

Time-dependent fragility curves are derived for both hospital units considering aging effects due to rebar corrosion following the analytical methodology presented in Pitilakis et al. [1]. Corrosion may affect an RC structure in a variety of ways (e.g. cover spalling, loss of steel-concrete bond strength, loss of steel cross sectional area) resulting to loss of ductility, reduction of load bearing capacity and finally to more brittle failure mechanisms. The aim of the present application is twofold: to apply the proposed methodology on a real building case and to compare the "time-building specific" fragility curves derived in the previous section with the time-dependent curves increasing the reliability of the methodologies and results.

The probabilistic model proposed by FIB- CEB Task Group 5.6 [72] is adopted for the computation of the corrosion initiation time, T_{ini}, due to chloride ingress. The statistical characteristics of the parameters involved in the computation of T_{ini} (Table 6) that are adopted in Pitilakis et al. [1] for a relatively high corrosion scenario are considered appropriate also for the coastal city of Thessaloniki. For a cover depth equal to 20mm, the mean value of T_{ini} is estimated approximately equal to 7 years. A 45-year corrosion scenario, which is considered representative of the current age of the hospital building units, is adopted in the present study. The chloride induced corrosion effects that are taken into account, are the section area loss of reinforced bars [73] and the concrete cover strength reduction ([74], [75]). The effects of corrosion are assumed to be distributed uniformly around the perimeter and along the concrete members. Table 7 summarizes the mean percentages (%) of reinforcement area loss and cover concrete strength reduction due to corrosion for the different RC elements of the structures under study within the elapsed time $(t\text{-}T_{ini})$. Results show that beams seem to be more affected regarding the steel area loss in comparison to

columns. On the other hand similar concrete cover reduction values are observed for both beams and column elements.

Table 6. Statistical characteristics of parameters affecting the chloride induced corrosion of RC elements adopted in the present study (after Pitilakis et al. [1]).

Parameter	Mean	Coefficient of variation (*cov*)	Distribution
Cover Depth (mm) α	20	0.40/0.32	Lognormal
Environmental function k_e	0.67	0.17	Normal
Chloride migration Coefficient ($D_{RCM,0}$) (m^2/s)	1.58E-11	0.20	Normal
Aging exponent n	0.362	cov=0.677 , a=0.0, b=0.98	Beta
Critical Chloride Concentration (C_{crit}) wt % cement	0.6	cov=0.25, a= 0.2, b=2.0	Beta
Surface Chloride Concentration (C_s) wt % cement	1.283	0.20	Normal
Rate of Corrosion (i_{corr}) mA/cm^2	2	0.25	Normal

Table 7. Loss of reinforcement (%) and concrete cover strength reduction (%) for the considered corrosion scenario (t=45 years).

	UNIT 1		**UNIT 2**	
	Steel area loss (%)	Concrete cover reduction (%)	Steel area loss (%)	Concrete cover reduction (%)
Beam	14	59	13	59
Column	8	59	8	56

4.2 Derivation of the time-dependent fragility curves and comparison with "time-building specific" curves

Using the seismic records of Table 5, IDA analysis is performed for the corroded building units following the same procedure as described in section 3.5 for the initial and updated models. The median IO limit value is defined based on the IDA results and is found equal to 0.1% for UNIT 1 and UNIT 2 respectively. The median of the defined CP values is estimated equal to 1.0% for both corroded units, which is a slightly lower value compared to the 1.1% estimated for the updated models. The assignments of the IO and CP limit states points on the IDA curves of the corroded units are presented in Fig. 14. The median PGA values for the two damage states are computed based on the regression analysis of Fig. 15 while the standard deviation is calculated accounting for the variability associated with the capacity of each structural type and the seismic demand.

The fragility curves of the initial, updated and corroded models of both UNIT 1 and UNIT 2 are compared in Fig. 16, while the fragility parameters (median and log-standard deviation) of the different cases are summarized in Table 8. As it can be seen the vulnerability of the structures increases over time due to corrosion, as expected. This increase is more noticeable for the CP limit state. Comparing the fragility between corroded and updated models, it is seen that for the IO limit state, no significant difference between

776 the curves is observed. For the CP state however, the curves corresponding to the corroded
777 models present a greater shift to the left in comparison to the respective curves of the
778 updated models indicating that the analytical procedure considering aging effects results to
779 higher fragility. In particular the difference in the median PGA values corresponding to the
780 CP state for the corroded models in relation to the updated ones is in the order of 9-13% for
781 UNIT 1 and UNIT 2. The 1978 Thessaloniki event is used again for the evaluation of the
782 damage probabilities for the different cases that are investigated. For the IO state (slight
783 damage level), no significant differences are observed in comparison to the initial state of the
784 building as the probability is high for all cases (approximately 95%). For the CP state
785 however the probability of occurrence is increased compared to the as built state of the
786 structure from 2% to 4% and 6% respectively for the updated and corroded case.

787

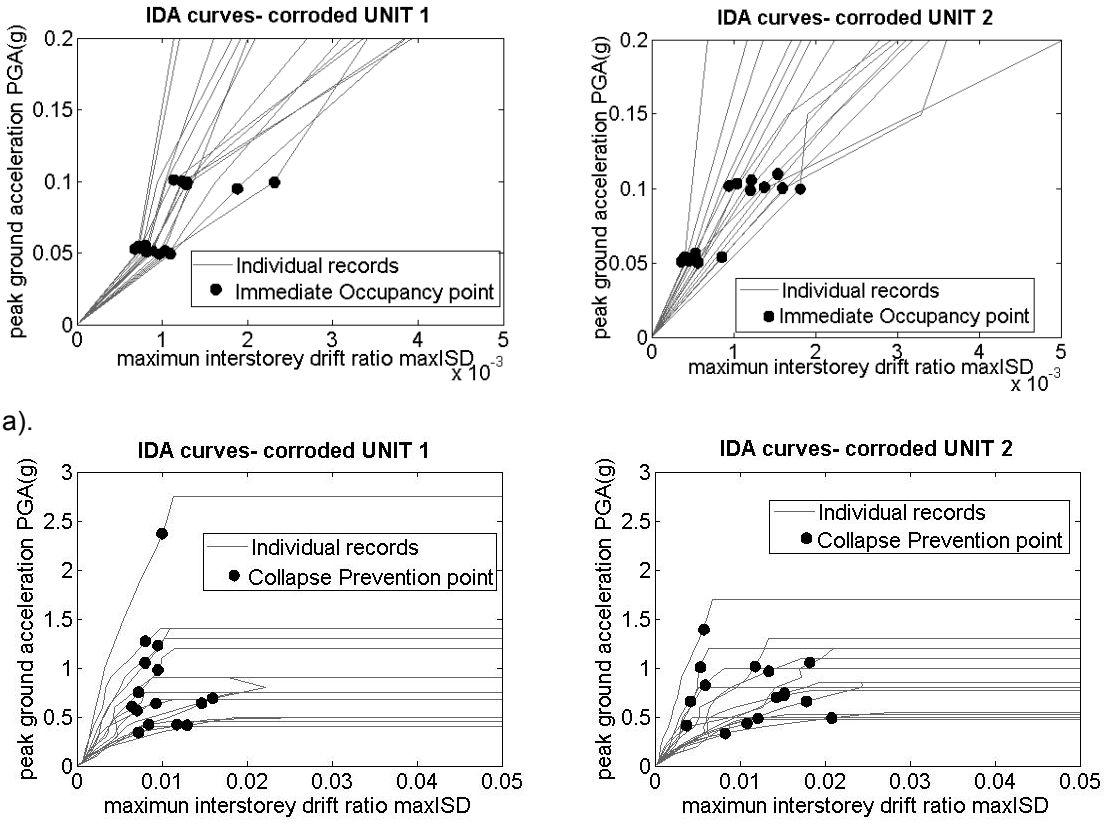

Fig.14. Assignments of the a): IO and b): CP limit damage state points on the IDA curves for the corroded units.

788

789

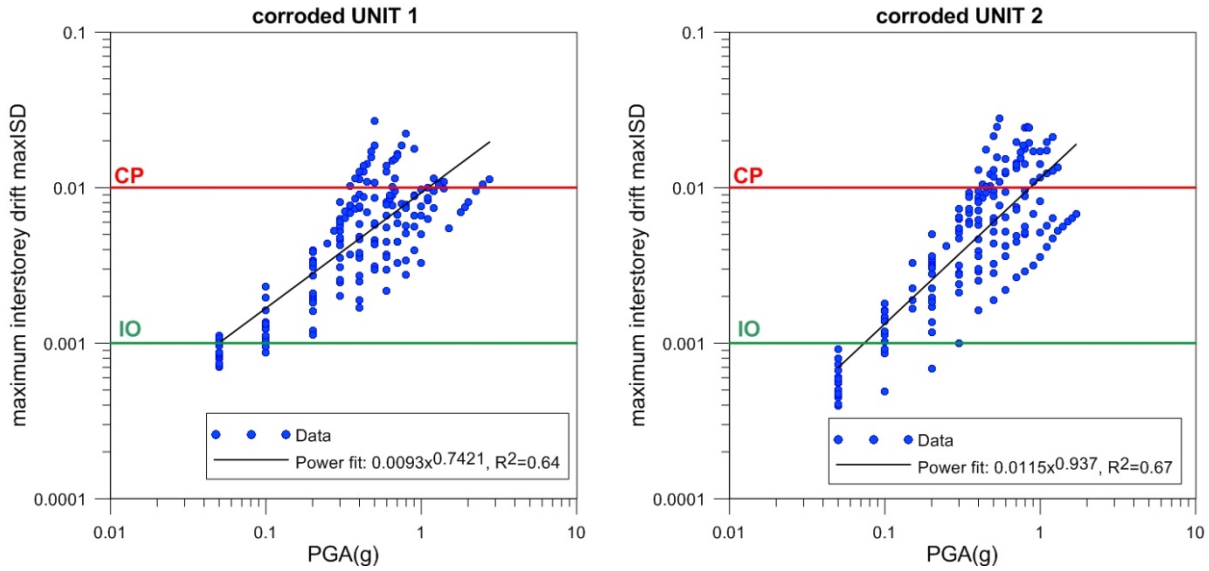

Fig.15. PGA-maxISD relationships for the corroded (t=45years) hospital buildings UNIT 1 and UNIT 2.

790

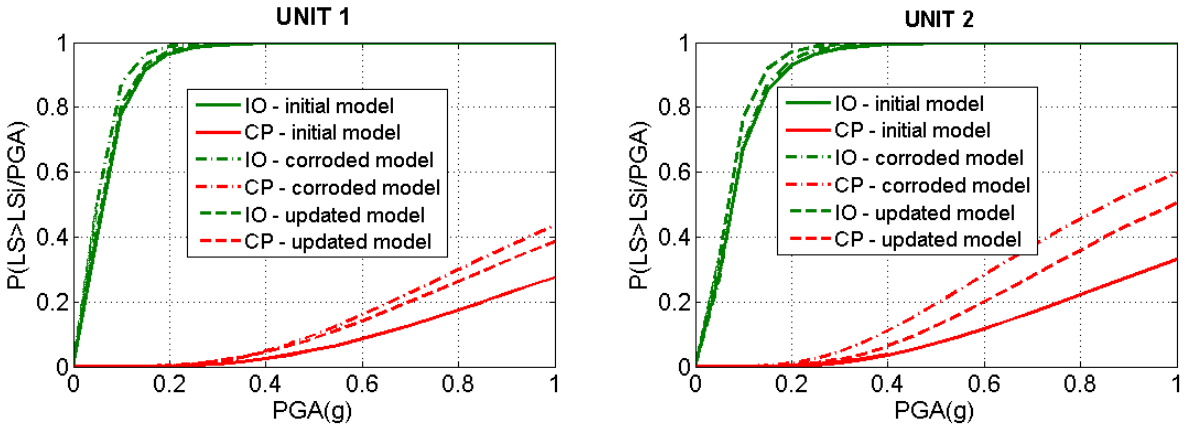

Fig.16. Comparative plots of the fragility curves corresponding to the initial, updated and corroded models of UNIT 1 and UNIT 2.

791

792

793 **Table 8.** Parameters of the derived fragility curves for the initial and updated finite element models for
794 UNIT 1 and UNIT 2.

RC building	Finite Element Model	Median PGA (g)		Dispersion
		IO	CP	
UNIT 1	Initial	0.059	1.49	0.67
	Updated	0.057	1.21	0.64
	Corroded	0.050	1.11	0.61
UNIT 2	Initial	0.074	1.35	0.68
	Updated	0.065	0.99	0.6
	Corroded	0.073	0.86	0.63

795

796

797

5. DISCUSSION - CONCLUSIONS

The “time-building specific” or actual seismic vulnerability of one of the main buildings of the most important hospital in Thessaloniki (AHEPA) has been assessed based on ambient noise field monitoring data. The special feature of the target building is that it is composed of two adjacent tall units that are connected with a structural joint. Ambient noise measurements were used to derive the experimental modal model of the two adjacent buildings first separately, and then for the entire building analyzed as one, taking into account the interaction of the two building units and identify their modal properties based on system identification and OMA respectively. The identified modal parameters were found very close for the different identification methods (non-parametric and parametric) applied as well as for the different system models analyzed, implying that the dynamic characteristics of the hospital building analyzed as one are possible to be captured by monitoring and analyzing the two adjacent buildings separately.

The modal identification results were used to update and better constrain the initial finite element models of the two adjacent units, which were based on the design and construction documentation plans provided by the Technical Services of the hospital. A sensitivity parameter related to the structural stiffness was adopted for the updating procedure, namely the compressive masonry infill strength. In general a good correlation with the experimental results was achieved for both building units.

Incremental dynamic analysis was performed for the initial and updated structural models to evaluate the seismic performance of the buildings when their actual state is taken into account. The fragility functions were derived for the IO and CP limit states in terms of PGA for both units. It was shown that the use of conventional generic fragility curves, although appropriate for assessing fragility and losses in a regional/urban scale, may lead to inaccurate fragility and loss estimates in the case of individual building assessment, which constitute crucial components in the framework of decision making and risk mitigation strategies (e.g. seismic safety and rehabilitation costs). Moreover, an overall increase in structures fragility for the updated models is observed in comparison to the ones corresponding to their initial state, which is attributed to deterioration phenomena affecting progressively the building over time. In order to increase the reliability of the derived results, the updated “time-building specific” fragility curves are compared with the time-dependent curves where aging effects due to rebar corrosion are taken into account through the analytical simulation of steel area loss and concrete cover strength reduction for a 45-year corrosion scenario adopting the methodology by Pitilakis et al. [1]. Although the applied methodologies are quite different approaches for assessing the actual structural condition, both result to an increase of the seismic vulnerability in comparison to the initial, “as built”

834 state of the hospital building. In general, a good correlation between the “time-building
835 specific” and time-dependent fragility curves is observed. The fact that for the CP state, the
836 structures’ fragilities appear to be higher for the corroded case may be attributed to the
837 relatively high rate of corrosion that was considered indicating that a moderate corrosion
838 scenario would be probably more appropriate for the hospital building case. In any case,
839 results indicate that potential degradation mechanisms that may affect the structural
840 condition over time should not be ignored especially in the case of buildings with strategic
841 interest (e.g. hospital) as this may lead to an underestimation of their real vulnerability
842 Overall this study provides further insight on the assessment of the “time-building
843 specific” seismic vulnerability of typical RC buildings using ambient noise field monitoring
844 data, presenting an integrated methodology where the actual state of the structure is taken
845 into account (degradation due to time, possible pre-existing damages, changes in geometry
846 and mass distribution, etc). Thus the presented methodology can be used to yield more
847 reliable structural models with respect to their real conditions in terms of structural detailing,
848 mass distribution and material properties. It should be noted herein that automated
849 operational analysis can be used to extract the modal properties of the building but also to
850 identify the role of environmental effects (e.g. degradation phenomena such as corrosion,
851 effect of temperature variation etc.) on the global behavior by tracking changes in modal
852 parameters with time ([76]; [77]; [78]). In order to quantify locally aging (corrosion) effects on
853 the RC elements, also non-destructive tests are required in order to gain insight regarding
854 the effects on a component level. Furthermore the proposed methodology should be
855 extended for “real-time” risk assessment and post-seismic fragility updating. As an example,
856 by exploiting the computing power of the strong motion sensing units installed in AHEPA, the
857 “time-building specific” fragility curves derived in this study allow the implementation of
858 building-customized alerting procedure suitable for performing an automatic building tagging
859 ([79], [80]). In this context, the use of field monitoring data will contribute in reducing the
860 uncertainties associated with the risk assessment procedure improving seismic safety and
861 allowing the development of robust real time assessment tools and appropriate risk
862 mitigation strategies.

863 **Acknowledgements**

864 The work reported in this paper was carried out in the framework of the REAKT
865 (http://www.reaktproject.eu/) project, funded by the European Commission, FP7-282862.
866 The seismic instruments used for the OMA analysis have been provided by the Geophysical
867 Instrument Pool Potsdam (GIPP). The temporary instrumentation array of 2013 was possible
868 thanks to the enthusiastic collaboration of the PhD students and part of the permanent staff
869 from SDGEE-AUTH. The authors are also very grateful to Tobias Boxberger for his help
870 during the temporary experiment. The staff of AHEPA hospital is acknowledged for their kind

support during the experiment. The authors want also to acknowledge the comments of the three reviewers, which significantly improved the quality of the paper.

References

1. Pitilakis KD, Karapetrou ST, Fotopoulou SD. Consideration of Aging and SSI effects on Seismic Vulnerability Assessment of RC Buildings. Bulletin of Earthquake Engineering, 2014a

2. Réveillère A, Gehl P, Seyedi D, Modaressi H. Development of seismic fragility curves for mainshock-damaged reinforced-concrete structures. Proceeding of the 15 WCEE, Lisboa, Sept. 2012

3. Pitilakis K, Crowley H, Kaynia, A. (Eds.). SYNER-G: Typology Definition and Fragility Functions for Physical Elements at Seismic Risk. Buildings, Lifelines, Transportation Networks and Critical Facilities, Series title: Geotechnical, Geological and Earthquake Engineering, 2014b; 27, DOI: 10.1007/978-94-007-7872-6.

4. Guéguen P, Michel C, Le Corre L. A Simplified Approach for Vulnerability Assessment in Moderate-to-low seismic hazard Regions: Application to Grenoble (France). Bulletin of Earthquake Engineering 2007; 5: 467–490.

5. Michel C, Guéguen P, Bard P-Y. Dynamic Parameters of Structures extracted from Ambient Vibration Measurements: An Aid for the Seismic Vulnerability Assessment of Existing Buildings in Moderate Seismic Hazard Regions. Soil Dynamics and Earthquake Engineering 2008;28:593–604.

6. Michel C, Guéguen P, Causse M. Seismic Vulnerability Assessment to Slight Damage based on Experimental Modal Parameters. Earthquake Engineering and structural dynamics 2012; 41: 81-98

7. Rainieri C, Fabbrocino G, Manfredi G, Dolce M. Robust output-only modal identification and monitoring of buildings in the presence of dynamic interactions for rapid post-earthquake emergency management. Engineering Structures 2012; 34:436-446.

8. Rainieri C, Fabbrocino G, Cosenza E. Near real-time tracking of dynamic properties for standalone structural health monitoring systems. Mechanical Systems and Signal Processing 2011;25: 3010-3026.

9. Rainieri C, Fabbrocino G. Automated output-only dynamic identification of civil engineering structures, Mechanical Systems and Signal Processing 2010; 24(3): 678-695, doi:10.1016/j.ymssp.2009.10.003.

10. Magalhaes F, Cunha A, Caetano E. Dynamic monitoring of a long span arch bridge. Engineering Structures 2008;30:3034-3044

11. Magalhaes F, Cunha A, Caetano E. Online automatic identification of the modal parameters of a long span arch bridge. Mechanical Systems and Signal Processing 2009;23:316-329

12. Picozzi M, Parolai S, Mucciarelli M, Milkereit C, Bindi D, Ditommaso R, Vona M, Gallipoli MR, Zschau J. Interferometric Analysis of Strong Ground Motion for Structural Health Monitoring: The Example of the L'Aquila, Italy, Seismic Sequence of 2009. Bulletin of the Seismological Society of America 2011;101: 635-651.

13. Lynch JP, Loh KJ. A summary review of wireless sensors and sensor networks for structural health monitoring. Shock and Vibration Digest, 2006;38(2):91-130.

14. Brownjohn JMW. Ambient vibration studies for system identification of tall buildings. Earthquake Engineering Structural Dynamics 2003; 32: 71-95.

15. Gentile C, Saisi A. Ambient vibration testing of historic masonry towers for structural identification and damage assessment. Construction and Building Materials 2007; 21(6):1311-21

16. Rainieri C, Fabbrocino G, Verderame GM. Non-destructive characterization and dynamic identification of a modern heritage building for serviceability seismic analyses. Independent Nondestructive Testing and Evaluation, 2013;60:17-31

17. Teughels A. Inverse modeling of civil engineering structures based on operational modal data. PhD thesis, Katholieke Universiteit of Leuven, 2003.

18. Jaishi B, Ren WX. Structural finite element model updating using ambient vibration test results. Journal of Structural Engineering 2005; 131: 617-628.

19. Zarate BA, Caicedo JM. Finite element model updating: multiple alternatives. Engineering structures, 2008; 30(12):3724-3730.

20. Savoia M, Vincenzi L, Bassoli E, Gambarelli P, Betti R, Testa R. Identification of the Manhattan bridge dynamic properties for fatigue assessment. Safety, Reliability, Risk and Life-Cycle Performance of Structure & Infrastructure 2013

21. Aras F, Krstevska L, Altay G, Tashkov L. Experimental and numerical modal analyses of a historical masonry palace. Construction and Building Materials, 2014;25:81-91

22. Antonacci E, De Stefano A, Gattulli V, Lepidi M, Matta E. Comparative study of vibration-based parametric identification techniques for a three-dimensional frame structure. Structural Control and Health Monitoring 2012; 19:579-608

23. De Stefano A. Structural identification and health monitoring on the historical architectural heritage. Key Engineering Materials 2007;347(1):37-54.

24. Peeters B. System Identification and Damage Detection in Civil Engineering. PhD thesis, Department of Civil Engineering, K.U.Leuven, 2000.

25. Farrar C, Doebling S, Nix D. Vibration-based structural damage identification. Philosophical Transactions of the Royal Society of London Series A-Mathematical, Physical & Engineering Sciences 2001; 359(1778):1674-1684.

26. Ramos LF, Marques L, Lourenco PB, De Roeck G, Campos-Costa A, Roque J. Monitoring historical masonry structures with operational modal analysis: Two case studies. Mechanical Systems and Signal Processing 2010;24:1291-1305

27. Goulet J A, C Michel and A Der Kiureghian “Data-driven post-earthquake rapid structural safety assessment”. Earthquake Engng Struct. Dyn. (2014) DOI: 10.1002/eqe.2541

28. Parloo E. Application of Frequency Domain System Identification Techniques in the Field of Operational Modal Analysis. PhD Dissertation, VRIJE Universiteit, Brussel, 2003.

29. Ewins D. Modal Testing: Theory and Practice. John Wiley and Sons, Inc., New York, 1984; 269 pp.

30. Allemang RJ. Analytical and Experimental Modal Analysis. UC-SDRLCN-20-263-662, 1994; 166 pp.

31. Heylen W, Lammens S, Sas P. Modal Analysis Theory and Testing. Katholieke Universiteit Leuven, Department of Mechanical Engineering, 1995

32. Reynders E. System Identification Methods for (Operational) Modal Analysis: Review and Comparison. Archives of Computational *Methods* in *Engineering, 2012; 19: 51-124.*

33. Bindi D, Petrovic B, Karapetrou S, Manakou M, Boxberger T, Raptakis D, Pitilakis K, Parolai S. Seismic response of an 8-story RC-building from ambient vibration analysis. Bulletin of Earthquake Engineering 2015; 13:2095-2120. doi: 10.1007/s10518-014-9713-y

34. Papazachos, B., D. Mountrakis, A. Psilovikos and G. Leventakis. Surface fault traces and fault plane solutions of the May-June 1978 shocks in the Thessaloniki area, North Greece, Tectonophysics, 1979; 53: 171 – 183.

35. Soufleris C, Jackson JA, King GCP., Spencer CP, Scholz CH. The 1978 earthquake sequence near Thessaloniki (northern Greece), Geophysical Journal of the Royal Astonomical Society 1982; 68, 429 – 458.

36. DIN 488, Reinforcing steel bars testing.

37. DIN 1045, Reinforced concrete structures – design and construction.

38. Strollo A, Parolai S, Jaeckel KH, Marzorati S, Bindi D. Suitability of short-period sensors for retrieving reliable H/V peaks for frequencies less than 1 Hz. Bulletin of the Seismological Society of America 2008; 98(2): 671-681.

39. Strollo A, Bindi D, Parolai S, Jaeckel KH. On the suitability of 1 s geophone for ambient noise measurements in the 0.1–20Hz frequency range: experimental outcomes. Bulletin of Earthquake Engineering 2008; 6(1): 141-147.

40. Vamvatsikos D, Cornell CA. Incremental dynamic analysis. Earthquake Engineering and Structural Dynamics 2002; 31.

41. Reynders E, Schevenels M., De Roeck G. MACEC 3.2: A Matlab toolbox for experimental and operational modal analysis-User's manual. Katholieke Universiteit, Leuven, 2011.

42. Van Overschee P, De Moor B. Subspace Identification for Linear Systems: Theory-Implemantation-Applications. K.U.Leuven Academic Publishers, 1996.

43. Rainieri C, Fabbrocino G. Operational modal analysis of civil engineering structures. Springer, New York; 2014

44. Allemang RJ, Brown DL . A Correlation Coefficient for Modal Vector Analysis. In: Proc of the 1st Intl Modal Anal Conf:01–18, 1982

45. Elnashai AS, Di Sarno L. Fundamentals of earthquake engineering. New York: Wiley; 2008.

46. Rainieri C, Fabbrocino G. Influence of model order and number of block rows on accuracy and precision of modal parameter estimates in stochastic subspace identification. International Journal of Lifecycle Performance Engineering 10, 2014;1(4):317-34.

47. Magalhães F, Cunha Á, Caetano E, Brincker R. Damping estimation using free decays and ambient vibration tests. Mechanical Systems and Signal Processing. 2010, 31;24(5):1274-90.

48. Rainieri C, Fabbrocino G, Cosenza E. Some remarks on experimental estimation of damping for seismic design of civil constructions. Shock and Vibration, 2010;17(4-5):383-95.

49. Mottershead JE, Friswell MI. Model Updating in Structural Dynamics: A Survey. Journal of Sound and Vibration 1993;167.

50. Scodeggio A, Monteiro R, Daccaro F, Crowley H, Pinho R. Finite Element Model Updating of Buildings using Dynamic Identification Measurements. Proceedings of 15WCEE, Lisboa, 2012.

51. Mazzoni S, McKenna F, Scott MH, Fenves GL. Open System for Earthquake Engineering Simulation User Command-Language Manual. Pacific Earthquake Engineering Research Center, Berkeley, California, 2009.

52. Mosalam KM, White RN, Gergely P. Static Response of Infilled Frames Using Quasi-Static Experimentation. ASCE Journal of Structural Engineering 1997; 123.

53. Paulay T, Priestley M. Seismic Design of Reinforced Concrete and Masonry Buildings. New York, 1992.

54. Popovics S. A Numerical Approach to the Complete Stress Strain Curve for Concrete. Cement and concrete research, 1973; 3(5):583-599.

55. Karsan I, Jirsa J. Behavior of Concrete under Compressive Loadings. ASCE Journal of the Structural Division 1969; 95:2543-2563.

56. Federal Emergency Management Agency (FEMA). Prestandard and Commentary for Seismic Rehabilitation of Buildings. Rep. FEMA-356, Washington, D.C., 2000.

57. CEN (2004) Eurocode 8: Design of structures for earthquake resistance - Part 1: general rules, seismic actions and rules for buildings. EN 1998-1:2004, European Committee for Standardization, Brussels.

58. Anastasiadis A, Raptakis D, Pitilakis K. Thessaloniki's detailed microzoning: subsurface structure as basis for site response analysis. Pure and Applied Geophysics 2001; 158: 2597-2633

59. Baker JW, Cornell CA. A Vector-Valued Ground Motion Intensity Measure Considering of Spectral Acceleration and Epsilon. Earthquake Engineering & Structural Dynamics. Stanford University, USA, 2005.

60. Iervolino I, Galasso C, Cosenza E. REXEL: computer aided record selection for code-based seismic structural analysis. Bulletin of Earthquake Engineering, 2010; 8.

61. Rossetto E, Elnashai A. Derivation of vulnerability functions for European-type RC structures based on observational data. Engineering Structures 2003; 25:1241-1263.

62. Wen YK, Song SH. Structural reliability/redundancy under earthquakes. ASCE Journal of Structural Engineering 2002; 129: 56–67.

63. De Luca F, Verderame GM. A practice-oriented approach for the assessment of brittle failures in existing reinforced concrete elements. Engineering Structures. 2013 Mar 31;48:373-88.

64. Vamvatsikos D, Cornell CA. Applied incremental dynamic analysis. Earthquake Spectra 2004; 20(2): 523-553.

65. Kwon OS, Elnashai AS. Probabilistic Seismic Assessment of Structure, Foundation and Soil Interacting Systems. NSEL Report Series, Report No. NSEL-004, 2007.

66. Selva J, Argyroudis S, Pitilakis K. Impact on loss/risk assessments of inter-model variability in vulnerability analysis. Natural Hazards 2013;67(2):723–746. doi:10.1007/s11069-013-0616-z

67. National Institute of Building Sciences. Direct physical damage – General building stock, HAZUS-MH Technical manual, Chapter 5. Federal Emergency Management Agency, Washington, D.C., 2004.

68. Perrault M, Gueguen P, Aldea A, Demetriu S. Using experimental data to reduce the single-building sigma of fragility curves: case study of the BRD tower in Bucharest, Romania. Earthquake Engineering and Engineering Vibration 2013; 12:643-658.

69. Kappos AJ, Panagiotopoulos C, Panagopoulos G, Panagopoulos El. WP4-Reinforced concrete buildings (Level I and II analysis), RISK-UE: An advanced approach to earthquake risk scenarios with applications to different European towns, 2003.

70. Kappos AJ, Panagopoulos G, Panagiotopoulos C, Penelis G. A Hybrid Method for the Vulnerability Assessment of R/C and URM Buildings. Bulletin of Earthquake Engineering 2006; 4: 391-419.

71. Penelis GG, Sarigiannis D, Stavrakakis E, Stylianidis KC. A statistical evaluation of damage to buildings in the Thessaloniki, Greece, earthquake of June, 20, 1978. Proceedings of 9th World Conference on Earthquake Engineering, Tokyo-Kyoto, Japan, August 1988.

72. CEB-FIB Task Group 5.6. Model for Service Life Design, fédération internationale du béton (fib), 2006.

73. Ghosh J, Padgett JE. Aging considerations in the development of time-dependent seismic fragility curves. Journal of Structural Engineering, 2010; 136(12): 1497-1511.

74. Coronelli D, Gambarova P. Structural assessment of corroded reinforced concrete beams: modeling guidelines. Journal of Structural Engineering, 2004; 130(8): 1214-1224.

75. Simioni P. Seismic response of reinforced concrete structures affected by reinforcement corrosion. PhD thesis. Faculty of Architecture, Civil Engineering and Environmental Sciences University of Braunschweig – Institute of Technology and the Faculty of Engineering University of Florence, 2009.

76. Peeters B, De Roeck G. One-year monitoring of the Z 24-Bridge: environmental effects versus damage events. Earthquake engineering & structural dynamics. 2001 Feb 1;30(2):149-71.

77. Yan AM, Kerschen G, De Boe P, Golinval JC. Structural damage diagnosis under varying environmental conditions—part I: a linear analysis. Mechanical Systems and Signal Processing. 2005a;19(4):847-64.

78. Yan AM, Kerschen G, De Boe P, Golinval JC. Structural damage diagnosis under varying environmental conditions—part II: local PCA for non-linear cases. Mechanical Systems and Signal Processing. 2005b;19(4):865-80.

79. Bindi D, Boxberger T, Orunbaev S, Pilz M, Stankiewicz J, Pittore M, Iervolino I, Ellguth E, and S Parolai. On-site early-warning system for Bishkek (Kyrgyzstan), Annals of Geophysics, 2015, in press.

80. Parolai S, Bindi D, Boxberger T, Milkereit C, Fleming K, Pittore M. On-Site Early Warning and rapid damage forecasting using 1 single stations: outcomes from the REAKT project, Seismological Research Letters, 2015, under revision.